

1                   **Temporal Variability in Gas Emissions at Bagana Volcano Revealed**  
2                   **by Aerial, Ground, and Satellite Observations**  
3

4 **B. T. McCormick Kilbride<sup>1,2</sup>, E. J. Nicholson<sup>3</sup>, K. T. Wood<sup>4</sup>, T. C. Wilkes<sup>5</sup>, C. I. Schipper<sup>6</sup>,**  
5 **K. Mulina<sup>7</sup>, I. Itikarai<sup>7</sup>, T. Richardson<sup>8</sup>, C. Werner<sup>9</sup>, C. S. L. Hayer<sup>1</sup>, B. Esse<sup>1</sup>, M. Burton<sup>1</sup>,**  
6 **T. D. Pering<sup>5</sup>, A. J. S. McGonigle<sup>5</sup>, D. Coppola<sup>10</sup>, M. Bitetto<sup>11</sup>, G. Giudice<sup>11</sup>, A. Aiuppa<sup>11</sup>**

7 <sup>1</sup>Department of Earth and Environmental Sciences, The University of Manchester, UK

8 <sup>2</sup>Centre for Crisis Studies and Mitigation, The University of Manchester, UK

9 <sup>3</sup>Department of Earth Sciences, University College London, UK

10 <sup>4</sup>Department of Mechanical, Aerospace & Civil Engineering, The University of Manchester, UK

11 <sup>5</sup>Department of Geography, University of Sheffield, UK

12 <sup>6</sup>Department of Earth Sciences, Victoria University of Wellington, NZ

13 <sup>7</sup>Rabaul Volcanological Observatory, PNG

14 <sup>8</sup>Department of Aerospace Engineering, University of Bristol, UK

15 <sup>9</sup>U.S. Geological Survey (contractor), New Plymouth, NZ

16 <sup>10</sup>Dipartimento di Scienze della Terra, Università di Torino, Italy

17 <sup>11</sup>Dipartimento di Scienze della Terra e del Mare, Università di Palermo, Italy

18 Corresponding author: Brendan T. McCormick Kilbride

19 ([brendan.mccormickkilbride@manchester.ac.uk](mailto:brendan.mccormickkilbride@manchester.ac.uk))

20

21 **Key Points:**

- 22       • We present the first measurements of volcanic gas composition at Bagana volcano.
- 23       • CO<sub>2</sub> and SO<sub>2</sub> fluxes at Bagana vary widely with levels of unrest, from ~10<sup>2</sup>-~10<sup>4</sup> td<sup>-1</sup>
- 24       • Unoccupied aerial systems (drones) are of great value in monitoring emissions from
- 25       inaccessible volcanic summits.
- 26

**Abstract**

28 Bagana is a remote, highly active volcano, located on Bougainville Island in southeastern Papua  
29 New Guinea. The volcano has exhibited sustained and prodigious sulfur dioxide gas emissions in  
30 recent decades, accompanied by frequent episodes of lava extrusion. The remote location of  
31 Bagana and its persistent activity have made it a valuable case study for satellite observations of  
32 active volcanism. This remoteness has also left many features of Bagana relatively unexplored.  
33 Here, we present the first measurements of volcanic gas composition, achieved by unoccupied  
34 aerial system (UAS) flights through the volcano's summit plume, and a payload comprising a  
35 miniaturised MultiGAS. We combine our measurements of molar CO<sub>2</sub>/SO<sub>2</sub> ratio in the plume with  
36 coincident remote sensing measurements (ground- and satellite-based) of SO<sub>2</sub> emission rate, to  
37 compute the first estimate of CO<sub>2</sub> flux at Bagana. We report low SO<sub>2</sub> and CO<sub>2</sub> fluxes at Bagana  
38 from our fieldwork in September 2019,  $\sim 320 \pm 76 \text{ td}^{-1}$  and  $\sim 320 \pm 84 \text{ td}^{-1}$  respectively, which we  
39 attribute to the volcano's low level of activity at the time of our visit. We use satellite observations  
40 to demonstrate that Bagana's activity and emissions behaviour are highly variable and advance the  
41 argument that such variability is likely an inherent feature of many volcanoes worldwide and as  
42 yet is inadequately captured by our extant volcanic gas inventories, which are often biased to  
43 sporadic measurements. We argue that there is great value in the use of UAS combined with  
44 MultiGAS-type instruments for remote monitoring of gas emissions from other inaccessible  
45 volcanoes.

46

**Plain Language Summary**

48 Bagana is a remote and highly active volcano in southeastern Papua New Guinea (PNG).  
49 Historically, it has been among the most active volcanoes in PNG, notable for its long-lived  
50 eruptions and sustained gas emissions. Bagana has only been infrequently studied before now.  
51 We used unoccupied aerial systems (drones) along with ground- and satellite-based remote  
52 sensing data to characterise the chemical composition and flux of Bagana's gas emissions and  
53 place these in the context of global volcanic emissions. Owing to low activity during the time of  
54 our fieldwork, we report lower than anticipated emissions of carbon dioxide and sulfur dioxide  
55 from Bagana. We argue that characterizing highly variable volcanic emissions is challenging  
56 without long-term continuous observations and that, for remote volcanoes like Bagana, both  
57 drones and satellite observations are powerful tools to undertake these observations.

58

59

## 60 **1 Introduction**

61 Bagana volcano, located on Bougainville Island in southeastern Papua New Guinea (6.137 °S,  
62 155.196 °E; 1855 m a.s.l.), is among the most active volcanoes on Earth with a record of semi-  
63 continuous lava extrusion stretching back to at least the mid-nineteenth century (Bultitude, 1976).  
64 Bagana may also be one of the youngest of Earth's active volcanoes; recent estimates suggest the  
65 modern edifice may have grown in only 300-500 years (Wadge et al., 2018). Satellite observations  
66 over the past two decades indicate that Bagana is a prodigious source of sulfur dioxide (SO<sub>2</sub>) gas  
67 into the atmosphere, with a mean annual emission rate of  $1379 \pm 89$  kt yr<sup>-1</sup> during 2005-15 (Carn  
68 et al., 2017). Bagana has been predicted to be a major emitter of volcanic carbon into the  
69 atmosphere (~6245 t d<sup>-1</sup>), based on global correlations between whole-rock Ba/La ratios and  
70 volcanic gas plume CO<sub>2</sub>/S<sub>T</sub> ratios (Aiuppa et al., 2019; Werner et al., 2019), but the chemical  
71 composition of Bagana's gas emissions has never before been measured directly.

72 The Bagana edifice is steep and unstable, and prone to rockfalls and debris avalanches (Bultitude,  
73 1976). The volcano cannot be climbed safely to deploy gas sensors directly in the plume (c.f.  
74 Aiuppa et al., 2005; de Moor et al., 2017). Recently, unoccupied aerial systems (UAS, or drones)  
75 have been used by volcanologists seeking to measure or sample gas emissions from remote or  
76 hazardous summits (McGonigle et al., 2008; Rudiger et al., 2018; Stix et al., 2018; Liu et al., 2019;  
77 Kazahaya et al., 2019; James et al., 2020; Pering et al., 2020; Liu et al., 2020a). Herein, we present  
78 the first measurements of volcanic gas chemistry at Bagana, achieved by flying a miniaturized gas  
79 sensing payload through Bagana's summit gas plume on-board a UAS. We also present  
80 simultaneously acquired remote sensing measurements of SO<sub>2</sub> emission rate. We calculate CO<sub>2</sub>  
81 emission rates by multiplying MultiGAS-measured CO<sub>2</sub>/SO<sub>2</sub> ratios by these SO<sub>2</sub> emission rates  
82 (de Moor et al., 2017; Werner et al., 2019).

83 Bagana's SO<sub>2</sub> emissions during our fieldwork (13-20 September 2019) were lower than the  
84 emission rates calculated from satellite observations in 2005-17 (McCormick Kilbride et al., 2019).  
85 Consequently, our calculated CO<sub>2</sub> emission rates for Bagana are rather lower than those predicted  
86 (Aiuppa et al., 2019). We evaluate these results in the context of changeable levels of activity at  
87 Bagana, as evidenced by multi-year satellite-based TROPOMI measurements of SO<sub>2</sub> emissions,  
88 and the possibility of shallow (i.e. hydrothermal) influences on volcanic gas emissions.

89 Our results support the developing paradigm that many, and perhaps most, of Earth's volcanoes  
90 exhibit wide variations in their gas emissions through time, which can hamper our ability to build  
91 volcanic emissions inventories based on short-duration field campaigns or assumptions regarding  
92 characteristic activity informed by historical trends (McCormick et al., 2015; de Moor et al., 2017;  
93 Werner et al., 2019). Remote volcanoes such as Bagana pose a challenge for the establishment  
94 of conventional monitoring networks, and therefore both UAS- and satellite-based methods will  
95 be valuable tools for characterising emissions in such settings.

96

97 **2 Data and Methods**

98 The key methods used in this study are remote sensing measurements (ground-based UV camera,  
99 UAS- and boat-based DOAS spectrometer traverses, satellite-based UV spectroscopy) of SO<sub>2</sub> flux  
100 and UAS-enabled in-plume measurements of volcanic gas composition (CO<sub>2</sub>/SO<sub>2</sub> molar ratio),  
101 using a MultiGAS sensor. CO<sub>2</sub> flux is computed from the product of SO<sub>2</sub> flux and CO<sub>2</sub>/SO<sub>2</sub> mass  
102 ratio.

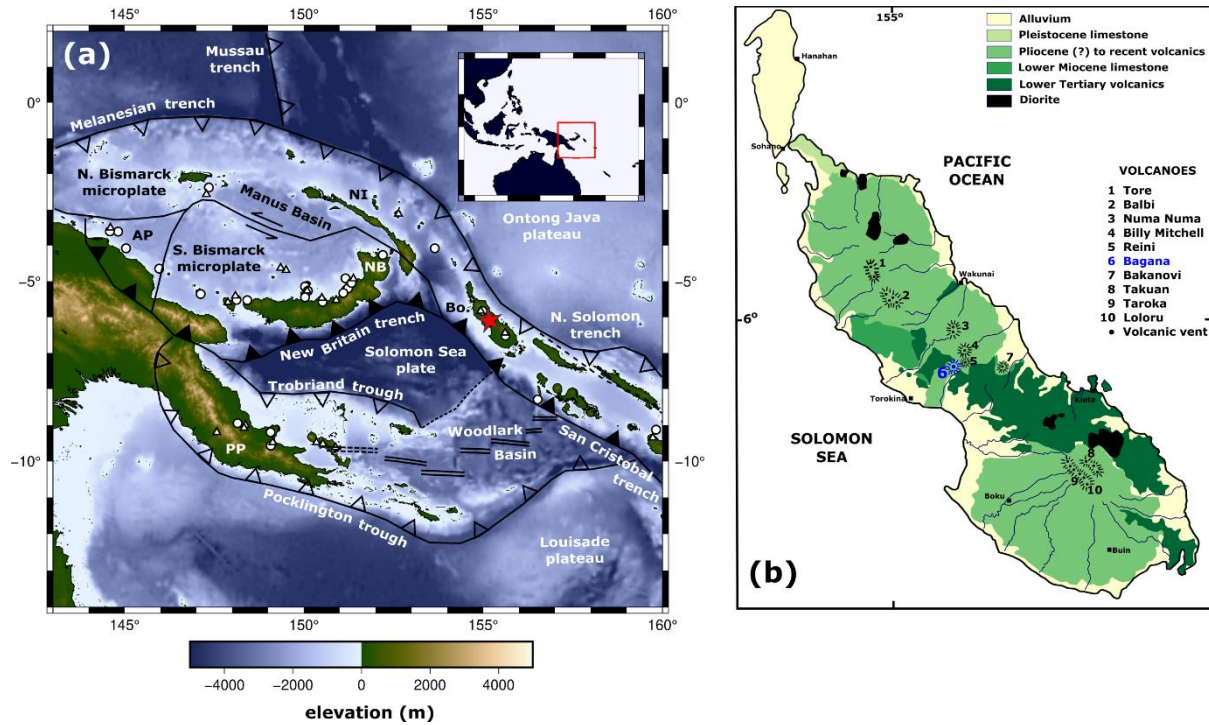
## 103 2.1 Geological Context

104 Bagana is one of seventeen post-Miocene volcanoes on Bougainville Island (Figure 1; Blake,  
105 1968). This volcanism is a consequence of plate convergence, with the Solomon Sea plate being  
106 subducted to the northeast beneath the Pacific plate (Holm et al., 2016). Bagana is a stratovolcano  
107 of basaltic andesite composition, sometimes described as a “lava cone”, being constructed largely  
108 of overlapping lava flows with relatively little pyroclastic material (Bultitude et al., 1978). The  
109 lava flows are rubbly with prominent marginal levees and steep fronts strewn with talus and fallen  
110 boulders. Block-and-ash flows and lahar deposits cover much of the lower northwestern slopes.

111 Bagana's characteristic activity comprises the alternation of extrusive eruptions persisting for  
112 several months and quiescent intervals dominated by voluminous passive degassing.  
113 Comprehensive reviews of Bagana's activity are provided by Bultitude (1976), Bultitude et al.  
114 (1978, 1981, 1981a) and, more recently, by Wadge et al. (2018) and McCormick Kilbride et al.  
115 (2019). The volume of the Bagana edifice is estimated to be 5.1-9.6 km<sup>3</sup>, depending on the  
116 (unknown) geometry of the underlying topography (Wadge et al., 2018). If the mean extrusion rate  
117 of 1.0 m<sup>3</sup> s<sup>-1</sup> calculated over the last 70 years is representative, the edifice may have been built in  
118 only 300-500 years. Intriguingly, the neighbouring pyroclastic shield volcano, Billy Mitchell,  
119 experienced a caldera-forming VEI 6 eruption 370 ± 19 years before present. Wadge et al. (2018)  
120 speculated that there may be a genetic link between caldera collapse and the cessation of activity  
121 at Billy Mitchell and the onset of lava extrusion and edifice construction at Bagana.

122 Measurements of Bagana's gas emissions consistently place it among the largest global volcanic  
123 SO<sub>2</sub> sources. Two recent studies used observations from the satellite-based Ozone Monitoring  
124 Instrument (OMI). Carn et al. (2017) reported a mean SO<sub>2</sub> flux of 1380 kt yr<sup>-1</sup> (3780 t d<sup>-1</sup>) in 2005-  
125 15. McCormick Kilbride et al. (2019) distinguished mean co-extrusive and quiescent SO<sub>2</sub> emission  
126 rates of 3300 t d<sup>-1</sup> and 2500 t d<sup>-1</sup> respectively, in 2005-17. Ground-based and airborne UV remote  
127 sensing measurements in the 1980s and 2000s found SO<sub>2</sub> emissions in the range of 2000-3200 t d<sup>-1</sup>  
128 (McGonigle et al., 2004; Andres and Kasgnoc, 1998). While no measurements have been made  
129 of CO<sub>2</sub> emissions from Bagana, Aiuppa et al. (2019) predicted a flux of 6245 ± 2335 td<sup>-1</sup>, based  
130 on the combination of Carn et al. (2017)'s reported SO<sub>2</sub> flux and an assumed CO<sub>2</sub>/S<sub>T</sub> of 2.4 ± 0.7.  
131 The latter ratio is based on global correlations between whole-rock Ba/La and volcanic gas plume  
132 CO<sub>2</sub>/S<sub>T</sub>, with Bagana posited by Aiuppa et al. (2019) to be a moderately carbon-rich system, with  
133 the local mantle wedge volatile budget being augmented by carbon released from sedimentary  
134 lithologies on the nearby subducting slab.

135

136  
137  
138139  
140  
141  
142  
143  
144  
145  
146  
147  
148  
149  
150

**Figure 1.** Left panel shows regional geology with key tectonic features marked, after Holm et al. (2016). Bagana is marked with the red star. AP = Adelbert Plate, NB = New Britain, NI = New Ireland, Bo. = Bougainville; PP = Papuan Peninsula. Active plate convergence is marked by black filled triangles; inactive convergent margins are indicated by open triangles. Topography and bathymetry is from the ETOPO1 Global Relief Model (<https://www.ngdc.noaa.gov/mgg/global/global.html>). Right panel shows Bougainville geological map, with major lithologies and volcanic edifices after Blake (1968).

151 Bagana erupts porphyritic basaltic andesite lavas with a phenocryst assemblage of augite,  
152 plagioclase and amphibole and a mean whole-rock  $\text{SiO}_2$  content of  $55.5 \pm 1.5$  wt. % (Bultitude et  
153 al., 1978). The volume of lava erupted over the last decade appears to be insufficient to supply all  
154 the gas emitted over the same interval, unless the melt sulfur concentration exceeds  $\sim 5000$  ppm,  
155 or alternatively the prodigious emissions are sourced from a deeper, non-erupted magma  
156 (McCormick Kilbride et al., 2019, Edmonds et al., 2022). At present, there are no petrological or  
157 geochemical data to place constraint on the volatile content of the magmas feeding Bagana's  
158 eruptions.

159  
160

## 161 2.2 UAS Gas Composition Flights

162 *Titan*. Our principal UAS is a fixed-wing aircraft, custom-built at the University of Bristol and  
163 based on the twin-propeller V-tail ‘Titan’ airframe from Skywalker (China). We used the Titan  
164 aircraft to make the the first measurements of gas composition at Manam volcano, also in Papua  
165 New Guinea, and for full details of the UAS configuration we refer the reader to Liu et al.(2020a)  
166 and Wood et al.(2020). Bagana represents a comparable target to Manam in terms of the required  
167 endurance (20-25 minute flights, with gas sensing measurements undertaken around 2000 m above  
168 take-off altitude and up to 7 km horizontal distance from take-off location).

169 We launched and recovered the Titan from the hamlet of Tsihokoa (6.159° S, 155.137° E, 150 m  
170 a.s.l.) in the Wakovi community, a small ridge above the Torokina river to the west of Bagana  
171 (Figure 2). We selected this site because it afforded a clear view of the volcano and plume, had a  
172 large open field available for our landing site, and enabled straightforward hand launch of the  
173 aircraft into the prevailing wind. To intercept the Bagana plume, we programmed automated flight  
174 paths with an altitude gain of 1700-2000 m and horizontal traverses of 7 km. We obtained  
175 permission for these beyond visual line of sight (BVLOS) flight operations from the Civil Aviation  
176 Safety Authority of Papua New Guinea. Our pre-programmed flight paths (example in Figure 2,  
177 full series available as a .kml file in Supplementary Material) comprised a sequence of waypoints  
178 between take-off, a zig-zag ascent path (with optimised ascent rate, climb angle, airspeed etc  
179 chosen based on our experience from previous campaigns), gas sensing over the volcanic summit,  
180 a glide back to the recovery area, and a loiter pattern for the aircraft to maintain until we could  
181 safely execute a manual landing. We developed our flight paths iteratively, combining a high-  
182 resolution topography model with our own observations of the volcanic summit and plume, both  
183 from the ground and from the FPV video stream. We made in-flight adjustments (switching to Fly-  
184 By-Wire mode) where necessary, based on real-time readouts from the on-board SO<sub>2</sub> gas sensor.  
185 This capability is valuable in that it allows a pilot to change mission targets during flight and also  
186 respond quickly to in-flight hazards.

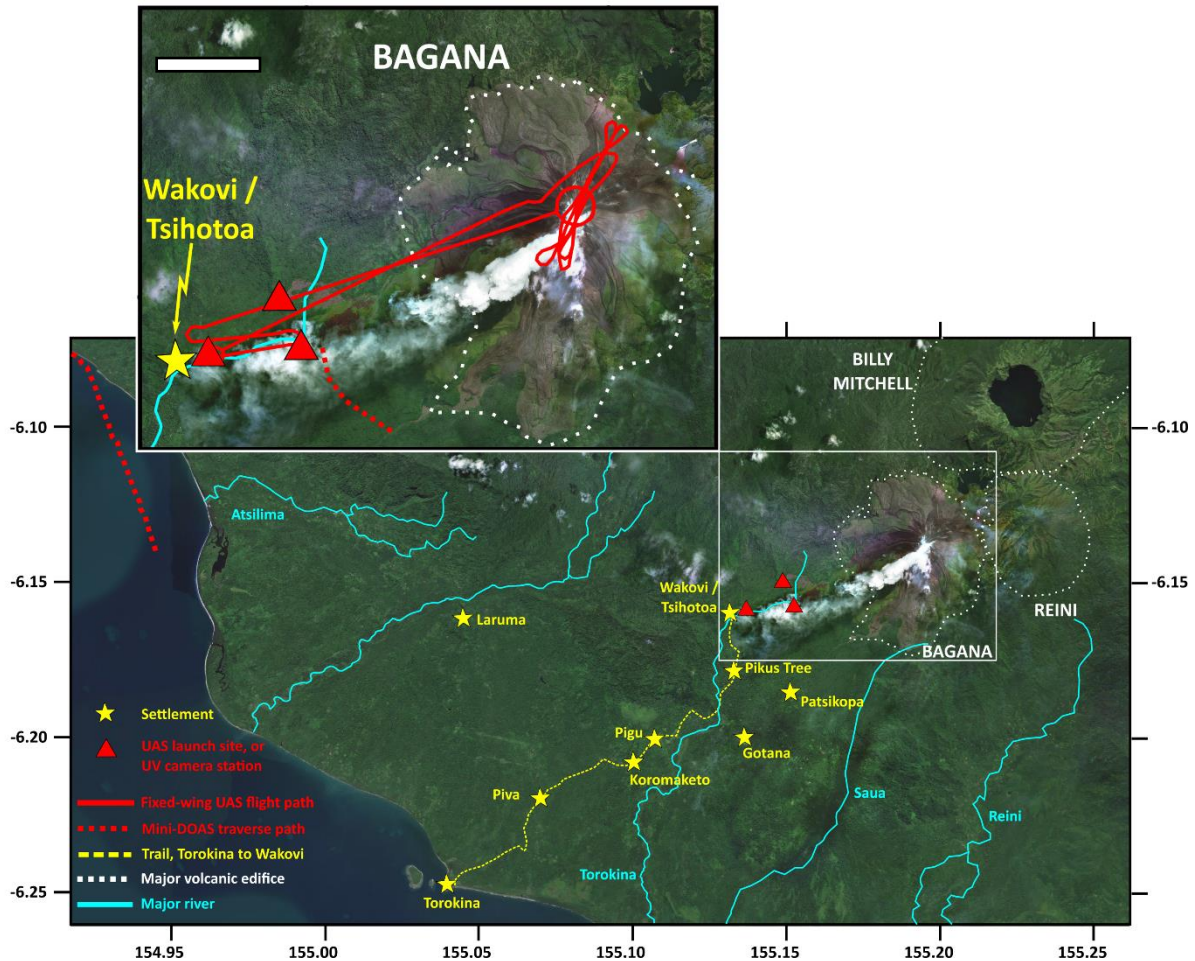
187 *MultiGAS*. The Titan carries a miniaturised MultiGAS sensor package in a fuselage payload bay.  
188 Our MultiGAS was built at the University of Palermo and is of the same configuration to those  
189 described in Liu et al.(2018), Pering et al.(2020) and Liu et al.(2020a). Air or gases are pumped (1  
190 L/min flow rate) through a 1- $\mu$ m particle filter to the sensors and data are logged at 1 Hz. We use  
191 SO<sub>2</sub> and H<sub>2</sub>S electrochemical sensors (City Technology T3ST/F-TD2G-1A and T3H-TC4E-1A,  
192 respectively), calibrated for 0-200 and 0-50 ppmv, respectively, with accuracy of  $\pm$  2% and  
193 resolution of 0.1 ppmv. There is a 13% SO<sub>2</sub> cross-sensitivity on the H<sub>2</sub>S sensors and, as described  
194 below, we did not detect H<sub>2</sub>S in the Bagana plume. We measure CO<sub>2</sub> concentration with a non-  
195 dispersive infrared spectrometer (Microsensorik Smartgas Modul Premium2), calibrated for 0-  
196 5000 ppmv with accuracy of  $\pm$  2% and resolution of 1 ppmv. To avoid radio interference from the  
197 UAS transmission system, we wrap the CO<sub>2</sub> spectrometer individually, and the whole sensor  
198 payload entirely, in brass foil. We calibrated the sensors with standard reference gases at the  
199 University of Palermo before and after the expedition, and found no evidence for sensor drift. Our  
200 on-board Bluedot BME280 sensor (pressure, temperature, humidity) and our backup both

201 malfunctioned due to rain infiltration during transits through cloud, and therefore we cannot  
202 calculate H<sub>2</sub>O concentration in the gas plume.

203 Each flight yields a time series of gas concentration for each sensor, which we post-processed  
204 using MATLAB® and Ratiocalc software (Tamburello, 2015). CO<sub>2</sub> concentrations were internally  
205 compensated for temperature ( $\pm 0.2\%$  full span per °C). We did not make any barometric pressure  
206 correction in the calculation of CO<sub>2</sub> concentration: our gas ratios are derived from relative changes  
207 in concentration and we flew the UAS at constant altitude during the plume interceptions (Flights  
208 4-6) for which we present data. We distinguish volcanogenic (or ‘excess’) CO<sub>2</sub> from atmospheric  
209 background, which we define as the mean CO<sub>2</sub> concentration measured during constant altitude  
210 flight in SO<sub>2</sub>-free air, updating the value for each flight. We measured no H<sub>2</sub>S concentrations  
211 exceeding the 13% cross-sensitivity of the sensor to SO<sub>2</sub> (determined during calibration with  
212 standard reference gases), and we therefore consider H<sub>2</sub>S undetected in the Bagana plume.

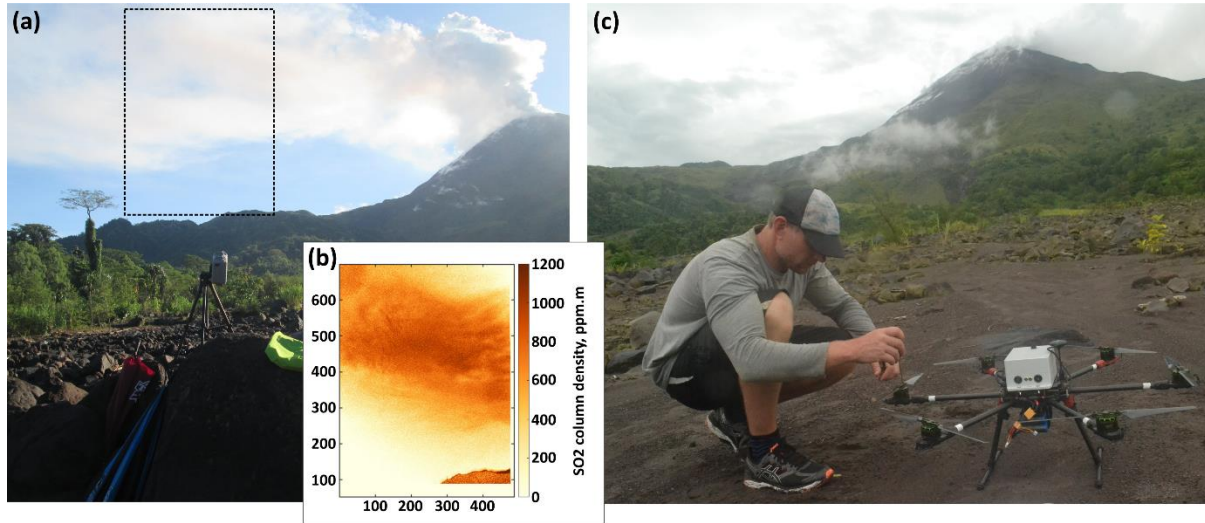
213 We account for different sensor response characteristics within the MultiGAS array by applying a  
214 Lucy-Richardson deconvolution algorithm to the CO<sub>2</sub> time series (Wood et al., 2019; Liu et al.,  
215 2020a; Pering et al., 2020). The algorithm is initiated using the measured time series and makes  
216 use of a sensor model determined empirically from the response of the NDIR to step changes in  
217 calibration gas concentration. The sensor model is best described by a windowed integral and is  
218 essentially an N-point moving average applied to the ‘true’ input signal: laboratory tests conducted  
219 by Wood et al. (2019) identified the CO<sub>2</sub> sensor to average over approximately 15 seconds, hence  
220  $N=15$ . The deconvolution effectively removes the sensor’s inherent filtering effect and the  
221 processed CO<sub>2</sub> concentration time series shows concentration peaks (i.e. plume intercepts) that are  
222 steeper, narrower and marginally greater in amplitude than the measured signal, without changing  
223 the integrated area beneath the peak. We calculate CO<sub>2</sub>/SO<sub>2</sub> ratios by fitting linear regressions to  
224 scatterplots of SO<sub>2</sub> concentration and our deconvolved CO<sub>2</sub> concentrations. The data selected for  
225 inclusion in each fitting are those measured by each sensor during ‘plume intercepts’, intervals  
226 where both SO<sub>2</sub> and CO<sub>2</sub> sensors record coincident concentration peaks as the UAS passes into,  
227 through, and beyond the volcanic gas plume. The horizontal speed of the Titan is  $\sim 20 \text{ ms}^{-1}$  and the  
228 duration of our plume intercepts range from  $\sim 30$ -70 seconds.

229

230  
231232  
233  
234  
235  
236  
237  
238  
239  
240

**Figure 2.** Satellite image (courtesy Bing Imagery) of Bagana surroundings with key locations from our fieldwork identified. We have omitted the flight paths shown in the inset from the main panel for clarity. Adjacent to Bagana are two dormant volcanoes, the pyroclastic shield Billy Mitchell with its summit crater lake and the deeply incised edifice Reini, probably of Pleistocene age. The representative fixed-wing UAS flight path shown corresponds to Flight 6. Paruata Island (Figure 4) is visible offshore from Torokina. Note that the plume shown here is characteristic of Bagana's emissions, which disperse generally towards the southwest, but this image was not acquired during our work in September 2019.

241  
242  
243  
244  
245  
246  
247  
248



249  
250  
251  
252  
253  
254  
255  
256

**Figure 3.** (a) View of Bagana and its gas plume from the UV measurement location ( $-6.158^{\circ}\text{S}$ ,  $155.152^{\circ}\text{E}$ ). Distance to volcano is around 4 km. Dashed box indicates the approximate field of view of the camera while acquiring data. (b) Representative absorption image, with darker colours indicating higher SO<sub>2</sub> column density. Ticks and labels on the left and lower edges of the images indicate the scale of the field of view, recorded in metres. (c) Crabcopter pre-flight checks. The miniDOAS spectrometer is housed in the grey box mounted on the upper surface of the UAS.

## 257 2.3 Ground-, UAS-, and Satellite-Based Remote Sensing

258 We measured SO<sub>2</sub> emission rates in the field using ultraviolet (UV) spectroscopy, with (1) zenith-  
259 pointing spectrometers (e.g. Galle et al., 2003; Kern et al., 2012) making traverses beneath the  
260 plume and (2) PiCam UV cameras (Wilkes et al., 2016, 2017). Following the field campaign, we  
261 studied SO<sub>2</sub> emissions from Bagana over longer intervals using the satellite-based spectrometer  
262 TROPOMI (Theys et al., 2019; Queisser et al., 2019, Burton et al., 2021).

263 *Spectrometer traverse measurements.* We made traverses by mounting spectrometers on both a  
264 second UAS and a boat. This UAS (the 'Crabcopter', Figure 3) is a multirotor aircraft under  
265 development at the Victoria University of Wellington. This expedition was the first field  
266 deployment of the aircraft, which is controlled via wireless link. The operator can view the  
267 progress of the aircraft in-flight via a video feed from the on-board action camera, telemetered to  
268 a tablet mounted on the ground control unit.

269 We flew exclusively manual (c.f. automated, pre-programmed) flights with the Crabcopter, aiming  
270 to make lateral traverses beneath the plume, flying at a steady altitude of 500 m above the ground,  
271 from a launch and recovery site at -6.158 °S, 155.152 °E, around 4 km from the volcano's summit.  
272 We were restricted to short observation windows (<1 hour) by persistent cloud cover and achieving  
273 a full traverse (i.e. passing from clean air, beneath the plume, and back to clean air) proved  
274 challenging due to the large width of the plume (>5 km). During our interval of best (clear-sky)  
275 measurement conditions, gas seemed to be ponding around the upper slopes of the edifice, making  
276 for large effective plume widths that came close to exceeding the Crabcopter's endurance. Our  
277 best traverse, on 17 September, was incomplete and to calculate an emission rate from this  
278 measurement we have had to make an assumption of plume symmetry.

279 We made further measurements by spectrometer while leaving the field area by boat on 20<sup>th</sup>  
280 September. We passed beneath Bagana's downwind plume to the southwest (30-40 km from  
281 summit, Figure 2); the plume was visible extending a great distance out to sea to our west. At this  
282 distance, the plume width was roughly 15 km.

283 The spectrometer payload is a miniature ultraviolet differential optical absorption spectrometer, or  
284 miniDOAS. The instrument quantifies the slant column concentration of a trace gas, here SO<sub>2</sub>, in  
285 its field of view, using scattered sunlight as a light source. The change in light intensity along a  
286 known path length due to absorption by SO<sub>2</sub>, relative to a blue-sky spectrum free of SO<sub>2</sub>, can be  
287 related directly to the SO<sub>2</sub> column concentration. Spectral data were acquired between 280 and 500  
288 nm at 0.6 nm resolution and at approximately 1 Hz using an Ocean Optics FLAME-S spectrometer,  
289 and the instrument position was tracked using a Ublox NEO-6M GPS receiver. From the vertical  
290 column densities we obtain in each plume traverse, we can calculate an integrated plume cross  
291 section of SO<sub>2</sub> concentration. Multiplication of this integrated section by the plume's speed (either  
292 from meteorological observations or a model value) provides us with an estimate of SO<sub>2</sub> emission  
293 rate. Here, we use wind data from GDAS, which is the National Center for Environmental  
294 Prediction (NCEP) Global Data Assimilation System ([https://www.ncdc.noaa.gov/data-  
295 access/model-data/model-datasets/global-data-assimilation-system-gdas](https://www.ncdc.noaa.gov/data-access/model-data/model-datasets/global-data-assimilation-system-gdas)). The emission rate  
296 error is determined by propagating the errors of the input parameters SO<sub>2</sub> column density, wind

297 speed and wind direction by assuming that the individual errors are independent of another. The  
298 error in the SO<sub>2</sub> column density is determined from the quality of the spectral fit.

299

300 *UV camera measurements.* The PiCam is built around two customised Raspberry Pi camera  
301 modules (Omnivision OV5647), modified via chemical removal of their Bayer filters to increase  
302 responsivity to UV radiation and remove the mosaic patten response (Wilkes et al., 2016, 2017).  
303 The PiCam field-of-view is  $23.1^\circ \times 17.3^\circ$  (width  $\times$  height). Each camera module is equipped with  
304 a bandpass filter (Edmund Optics Inc.), one centred at 310 nm and the second at 330 nm (each  
305 with 10 nm bandpass full-width-at-half-maximum), which are, respectively, typical on- and off-  
306 bands for the detection of SO<sub>2</sub> (Mori and Burton, 2006). The cameras, Raspberry Pi 3 Model B  
307 computers for interfacing, batteries and a GPS unit are housed in a Pelicase. We manage data  
308 capture via custom Python 3 code (Wilkes et al., 2016, 2017).

309 We carried out image processing after acquisition, not in real-time, and again using custom Python  
310 3 code. Gliss et al. (2017) have reviewed SO<sub>2</sub> camera image processing techniques in detail; we  
311 primarily use the protocols outlined by Kantzas et al. (2010). Our images are all dark image  
312 corrected and we correct for vignetting using a clear-sky mask acquired in the field. To assess  
313 clear-sky background intensity we measure the average intensity of light in a region of sky close  
314 to the plume without volcanic gas. We calibrated our apparent absorbance images using three gas  
315 cells of known SO<sub>2</sub> column densities (0, 412 and 1613 ppm.m). The column densities we measured  
316 during the field campaign were all within this calibration range, therefore we were not required to  
317 extrapolate to higher values. We extracted integrated column amounts from a line perpendicular  
318 to plume transport (Figure 3) and calculated plume speed with the cross-correlation technique  
319 (Mori and Burton, 2006). The prevailing environmental conditions were extremely challenging for  
320 UV spectroscopy, with high atmospheric water vapour, persistent cloud cover throughout each day  
321 from around 0900 onwards and relatively low UV levels during the early morning and late  
322 afternoon clear-sky intervals. Our period of best quality acquisition comprised around one hour on  
323 the morning of 18 September.

324 Assuming a 10% uncertainty in our estimated distance from the PiCam to the plume, the estimated  
325 distance between integrated column lines for cross-correlation has a corresponding uncertainty of  
326 10%. This translates to a 10% uncertainty in wind speed estimation. We calculated the integrated  
327 column amount uncertainty using the PiCam's detection limit of the system, estimated as 180  
328 ppm.m following the method of Kern et al. (2010). Using this as the SO<sub>2</sub> column amount  
329 uncertainty and summing in quadrature across each pixel of the integrated column gives an overall  
330 integrated column uncertainty (Wilkes et al., 2017). Our measurement geometry, with a vertically  
331 spread plume at a relatively close distance, precluded the inclusion of a hillside in our UV images,  
332 which precluded the use of Champion et al. (2015)'s image-based correction for light dilution.  
333 Given our distance of around 3 km to the plume, we favour a conservative estimate of 20%  
334 uncertainty arising from light dilution (Champion et al., 2015). We estimate the cell calibration  
335 uncertainty to be 10%, following the manufacturer quoted uncertainty of the gas cell column

336 amounts. Summing all uncertainties in quadrature, our SO<sub>2</sub> camera data are subject to a total  
337 uncertainty of 0.7-1.2 kgs<sup>-1</sup>, or ≈25% (Figure 8a).

338

339 *Satellite observations.* The Tropospheric Monitoring Instrument, TROPOMI, is a hyperspectral  
340 imaging spectrometer carried by the European Space Agency (ESA)'s Sentinel-5 Precursor (S-5P)  
341 satellite (Veefkind et al., 2012). Launched in 2017 and operational since April 2018, TROPOMI  
342 had a spatial resolution of  $7 \times 3.5 \text{ km}^2$  (thirteen times better than the earlier Ozone Monitoring  
343 Instrument, OMI), which was improved to  $5.5 \times 3.5 \text{ km}^2$  in August 2019. This fine spatial  
344 resolution has enabled the mapping of atmospheric SO<sub>2</sub> concentrations with unprecedented detail,  
345 in turn enabling the most comprehensive overview yet of volcanic outgassing as observed from  
346 space, including monitoring of SO<sub>2</sub> emission rates in both syn- and inter-eruptive episodes at sub-  
347 daily temporal resolution (Theys et al., 2019; Quei er et al., 2019).

348 In this study we use the COBRA (Covariance-Based Retrieval Algorithm) Level 2 SO<sub>2</sub> TROPOMI  
349 dataset (<https://distributions.aeronomie.be>, accessed Feb. 2022; Theys et al., 2021). We calculated  
350 SO<sub>2</sub> emission rates from TROPOMI using the PlumeTraj analysis toolkit (Quei er et al., 2019;  
351 Burton et al., 2020). The toolkit, written in Python 3, uses the HYSPLIT trajectory model (Draxler  
352 & Hess, 1998), to calculate backward trajectories for all pixels in the satellite field of view with  
353 confirmed detection of volcanic SO<sub>2</sub>. Wind shear within the atmosphere causes trajectories at  
354 different altitudes to move at varying speeds and directions; thus we can isolate those that intersect  
355 with the source volcano.

356 To remove noise from our quantification of SO<sub>2</sub> emission rates, we perform two initial  
357 thresholding tests on each pixel: 1) the SO<sub>2</sub> concentration must exceed three times the random  
358 noise for that pixel; 2) two of the surrounding eight pixels must also pass this test, removing  
359 spurious high concentration pixels. We run all pixels that pass these thresholding tests through the  
360 PlumeTraj trajectory analysis. We assign the trajectory that passes closest to the volcano as the  
361 optimal trajectory for that pixel, discarding the pixel if the approach distance exceeds 250 km. This  
362 optimal trajectory gives us the altitude at the time of measurement, the injection altitude, and the  
363 injection time. Since the SO<sub>2</sub> vertical column density (VCD, i.e. concentration) is dependent upon  
364 the plume's altitude, raw TROPOMI data are provided assuming three altitudes (1, 7, and 15 km).  
365 We use a linear interpolation between these prescribed altitudes to obtain a corrected concentration  
366 for each pixel. We multiply this concentration by the pixel area to give the SO<sub>2</sub> mass which, when  
367 combined with the injection time and performed for all pixels in the plume, yields an emission flux  
368 time series. We can then average this flux time series to give a daily emission rate, which is  
369 reported within this study, along with the peak 1-hour emission rate for each day.

370 In addition to our PlumeTraj analysis, we calculate monthly mean emission rates (expressed as  
371  $\text{td}^{-1}$  for each month of the study interval) by regridding and averaging the 1 km COBRA  
372 TROPOMI data. Our method follows Theys et al. (2021), using only high-quality pixels (i.e. we  
373 discard the outermost 25 pixels from both edges of the swath, those with a cloud fraction >30%,  
374 or those with a solar zenith angle >60°) and performing spatial averaging using a 10-point box  
375 car average. We stack the regridded data and then divide by the number of positive detections  
376 within each grid box. We perform the mass calculation for a 4° box centred on Bagana, with the  
377 averaged VCD from each grid box multiplied by its area and then summed. This approach also

378 provides maps of monthly mean SO<sub>2</sub> VCD over the study region (Figure 10, Supplementary  
379 Figure 5).

380 We present the satellite time series for two reasons: (i) to affirm an order of magnitude agreement  
381 between ground- and space-based observations of Bagana's SO<sub>2</sub> emissions, and (ii) to interrogate  
382 the long-term trend of emissions since 2017 to the present (i.e. since the analysis of McCormick  
383 Kilbride et al., 2019). Rigorous ground-truthing of the satellite data product is not a key goal of  
384 our study due to the limited availability of our ground-based data and the challenging measurement  
385 conditions we faced (low UV, short observation windows). Moreover, recent efforts to reconcile  
386 ground-based remote sensing measurements with emission rates retrieved from TROPOMI data  
387 have already demonstrated the potential for good agreement and robust inter-comparison (Theys  
388 et al., 2019; Queisser et al., 2019).

389 We also show infrared data from the Moderate Resolution Imaging Spectroradiometer  
390 (MODIS) instrument, processed using the volcanic hotspot detection system MIROVA developed  
391 by Coppola et al. (2016, 2020). MODIS provides data in the mid-infrared (MIR: 3.44-4.13  $\mu\text{m}$ )  
392 about four times per day (two at night and two during the day) at a resolution of 1 km. Incandescent  
393 material on the Earth's surface (e.g. lava, whether in flows, domes or lakes) is a strong source of  
394 thermal energy in the MIR region of the electromagnetic spectrum, a feature which is used by the  
395 MIROVA algorithm to detect the presence of sub-pixel hot sources. The level of MIR radiance  
396 above that of the surrounding 'background' landscape is then used to calculate the Volcanic  
397 Radiant Power (VRP), a combined measurement of the area of the volcanic emitter and its effective  
398 radiating temperature (Coppola et al., 2016). MODIS data is particularly valuable at Bagana as a  
399 direct indicator of active lava extrusion (e.g. Wadge et al., 2012, 2018; McCormick Kilbride et al.,  
400 2019).

401

402

403

404 **3 Results**

## 405 3.1 Volcanic Activity

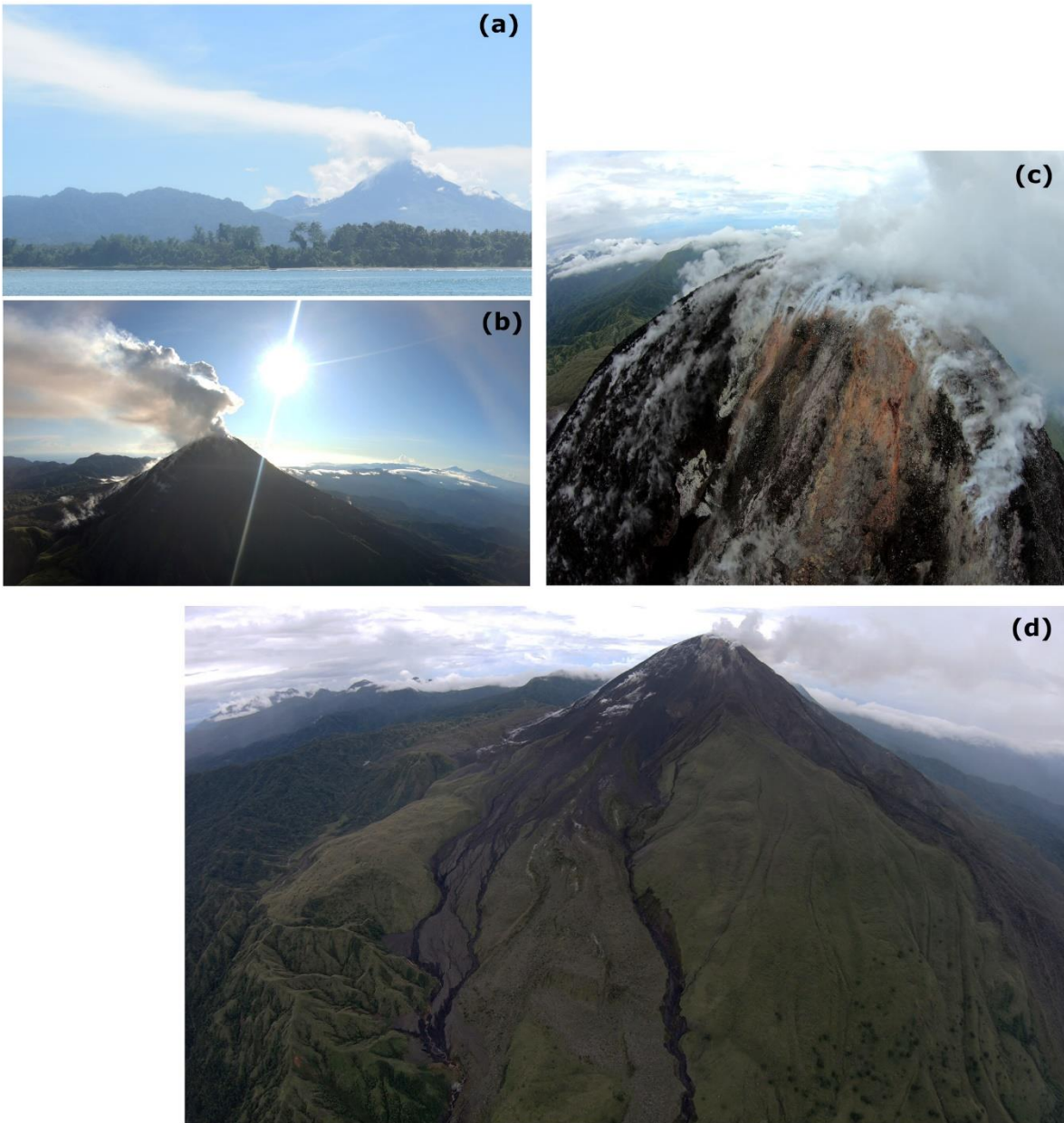
406 Bagana was not evidently erupting when we visited in September 2019. Past observations indicate  
407 that lava flows are sluggish and that active effusion may be better identified by rockfalls. We  
408 observed no incandescence on either summit or flanks and witnessed no ash venting (c.f.  
409 McCormick Kilbride et al., 2019). The only evidence of recent eruptive activity was a strongly  
410 steaming lava flow on the northern flank, which we observed on arrival in the area by boat and  
411 from Piva Government Centre, our first basecamp (Figure 4a, Figure 2). Ephemeral steam  
412 emissions are common across the edifice, most likely the result of rainwater evaporating. The  
413 persistence of the steaming from the northern flank lava flow may indicate some residual magmatic  
414 degassing or simply the current hottest point on the volcano's surface. This flow was probably  
415 erupted during an interval of sustained thermal anomalies detected by MIROVA satellite  
416 observations in July-December 2018 (Global Volcanism Program, 2019a-c). Specifically, a short  
417 period of effusive activity may have occurred around 6 August 2019, when a peak in radiative  
418 power over Bagana was detected by the MODIS satellite and a weak thermal anomaly was  
419 observed by Sentinel-2 (Massimetti et al., 2020;  
420 [https://www.mirovaweb.it/?action=volcanoDetails\\_S2&volcano\\_id=255020](https://www.mirovaweb.it/?action=volcanoDetails_S2&volcano_id=255020)).

421 Throughout our fieldwork, we observed sustained, dense white emissions from Bagana's summit,  
422 with the plume visibly extending several kilometres over the ocean to the west of Bougainville  
423 Island (Figure 4a). From images captured by the Titan's on-board action camera, we saw that the  
424 plume is composed of emissions escaping from numerous points on the edifice. There is a dense  
425 concentration of fumaroles around the summit and more subdued emissions from the fresh lava  
426 flow on the northern flank (Figure 4b, Supplementary Figure 1). The majority of the emissions  
427 originate from the summit, which is encrusted with white, grey and yellowish mineral deposits  
428 (Figure 4c).

429 Residents of the Wakovi community (Figure 2) reported that no substantial explosive activity has  
430 occurred at Bagana since 2014, when hot ashfall ignited house roofs and the community  
431 schoolhouse and resulted in temporary self-evacuations to communities near the coast. Villagers  
432 reported a number of lines of evidence by which they infer imminent eruptions including  
433 vegetation dieback along the upper reaches of the Torokina River due to rising water temperature,  
434 presumably a result of heat transfer from rising magmas. The principal risk to the local community  
435 results from debris avalanches, including lahars, locally called *tovure*, which pass from the edifice  
436 slopes into the upper reaches of the Torokina river. As with our previous visit in 2016, the western  
437 approaches to the volcano are covered in thick debris flow deposits, quite distinct from both recent  
438 and historic lava flows (Figure 4d).

439

440



441  
 442 **Figure 4.** (a) View of Bagana and its large gas plume from Paruata Island on 15 September 2019 (Figure 2), around  
 443 22 km southwest of the summit. The steaming 2018 lava flow can be seen descending the left flank of the volcano,  
 444 abutting against the small dome on the skyline. (b) A northeast-ward view from the Titan's forward-facing action  
 445 camera, taken during the approach to the volcano in Flight 6. Note the strong vertically-rising gas plume and the  
 446 2018 lava flow, steaming on the lower left of the image. (c) The summit of the volcano, with extension mineral  
 447 precipitation and abundant fumaroles. (d) A view from the forward-facing action camera, taken during the approach  
 448 to the volcano in Flight 4, illustrating the different deposits mantling the edifice. In the lower centre of the image is a  
 449 large braided lava flow with a rubbly surface that erupted in 2010-12. To the left is a narrow channel of debris  
 450 avalanche or lahar deposits, which extends several hundred metres further west (behind the aircraft's northeast-ward  
 451 viewing direction). On the right of the 2010-12 lava flows is a heavily vegetated suite of lava flows erupted from  
 452 1957-66 (Wadge et al., 2012). At the extreme right of the image are unvegetated rubbly flows mostly erupted in  
 453 2000-05. The lava flows all exhibit prominent channel/levee structures.

454

### 3.2 Gas Composition

455 We made seven flights over Bagana's summit with the Titan UAS and encountered the gas plume  
456 on Flights 4, 5 and 6. We have described all flights fully in our Supplementary Material, discussing  
457 planned and realised flight paths and describing the plume intercepts in terms of peak gas  
458 concentrations and the topology of the gas concentration time series. We also discuss different  
459 means of deriving CO<sub>2</sub>/SO<sub>2</sub> ratios across each flight, with the resulting ratios all presented in Table  
460 1. In Figure 5, we show the molar CO<sub>2</sub>/SO<sub>2</sub> ratio for each plume intercept, grouped by flight, and  
461 plot these ratios as a function of plume exposure time and peak SO<sub>2</sub> concentration. In Figure 6, we  
462 show the full CO<sub>2</sub> and SO<sub>2</sub> concentration time series measured by our MultiGAS during Flight 6  
463 and the CO<sub>2</sub>–SO<sub>2</sub> scatterplots we used to derive CO<sub>2</sub>/SO<sub>2</sub> ratios for Flight 4, Flight 5, and Flight  
464 6. In Figure 7, we plot CO<sub>2</sub> and SO<sub>2</sub> concentrations along the Titan flight path during Flight 6. The  
465 full timeseries for Flight 4 and 5 are in Supplementary Figure 2 and the gas concentrations along  
466 the flight paths for these flights are in Supplementary Figure 4.

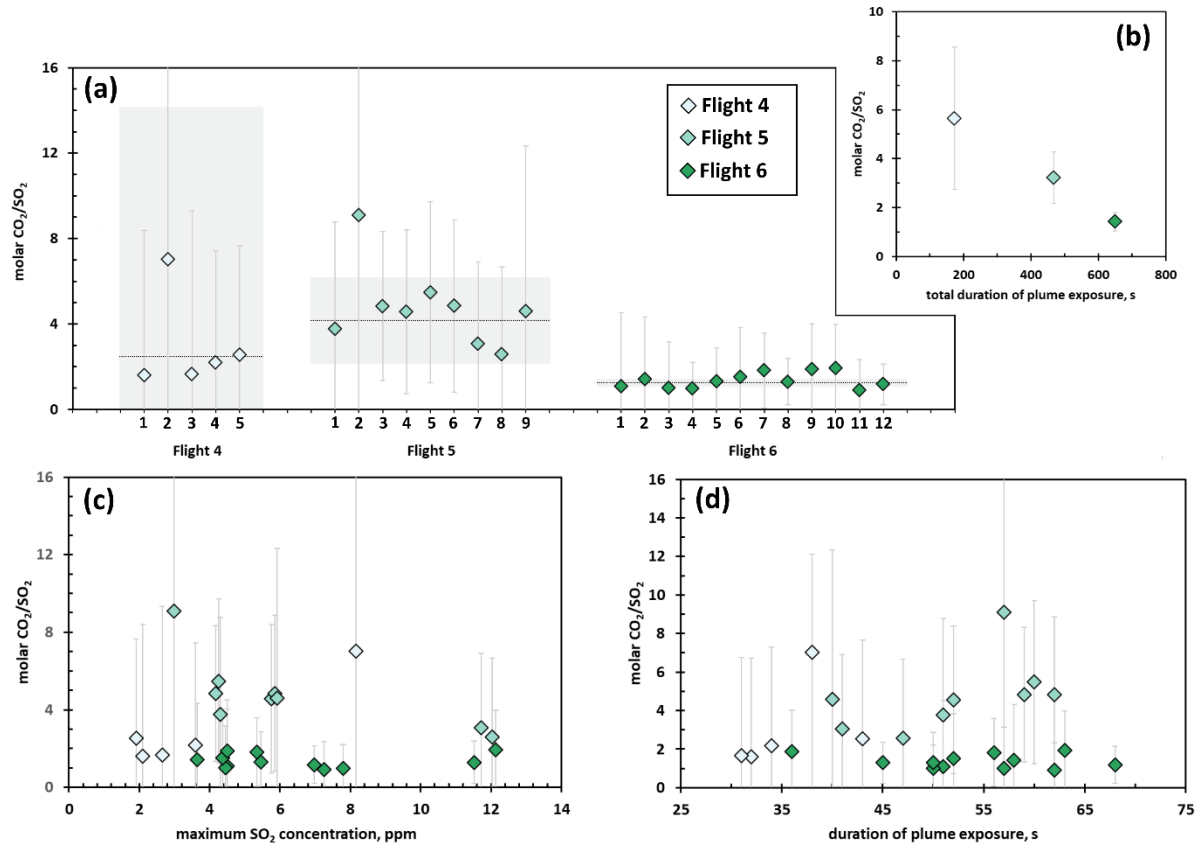
467 Figure 5a shows the CO<sub>2</sub>/SO<sub>2</sub> ratios we calculate for individual plume intercepts. These vary  
468 widely and are subject to large uncertainties, due to the low concentrations of gas that the Titan  
469 encountered and the short duration of sensor exposure to the volcanic plume. We do not see strong  
470 correlations between per-intercept CO<sub>2</sub>/SO<sub>2</sub> ratios and peak SO<sub>2</sub> concentration (Figure 5c) or  
471 exposure time (Figure 5d). In Flight 6, our per-intercept ratios remained relatively stable across a  
472 range of SO<sub>2</sub> concentration and time spent in the plume, while Flights 4 and 5 show more internal  
473 variability. We do see significantly lower errors on the ratios calculated across each flight as the  
474 duration of gas-sensor contact increased (Figure 5b). We see no evidence for systematic spatial  
475 variations in plume composition (Supplementary Figure 3, 4). Our measured SO<sub>2</sub> and excess CO<sub>2</sub>  
476 concentrations tend to be higher when the UAS was closer to the volcano's summit, but there is  
477 no correlation between distance to the summit and instantaneous CO<sub>2</sub>/SO<sub>2</sub> molar ratio.

478 To derive Bagana's CO<sub>2</sub> emission rate (see below), we multiply SO<sub>2</sub> emission rates measured via  
479 UV remote sensing by a representative CO<sub>2</sub>/SO<sub>2</sub> ratio. The ratio we calculate from our Flight 6  
480 data is subject to lower errors than the Flight 4 and 5 ratios (Table 1) and there is less variation in  
481 the per-intercept ratios within Flight 6 (Figure 5a). However, the Titan did unambiguously  
482 encounter the volcanic plume several times across Flights 4 and 5. We cannot rule out that the  
483 differences in gas composition between each flight are genuinely reflecting spatial or temporal  
484 variations in plume chemistry, rather than being consequences of our sampling approach.  
485 Therefore, we consider that the overall CO<sub>2</sub>/SO<sub>2</sub> ratio should be based on as much of our data from  
486 these three successful flights as possible. If we combine Flights 4-6 and fit a single linear  
487 regression through the data, we obtain CO<sub>2</sub>/SO<sub>2</sub> of  $2.4 \pm 0.6$ . Alternatively, we can calculate a  
488 weighted mean CO<sub>2</sub>/SO<sub>2</sub> ratio of  $1.6 \pm 0.2$  from our (n=26) individual plume intercepts, weighting  
489 our calculation according to the error on each intercept, aiming to limit the influence of highest  
490 uncertainty data on the overall 'representative' ratio. This is to establish mean CO<sub>2</sub>/SO<sub>2</sub> only, and  
491 not to disregard potential temporal variations in composition between flights. Filtering the data to  
492 calculate a ratio from plume intercepts where SO<sub>2</sub> concentration exceeded 5 ppm (n=12) and 10  
493 ppm (n=4), yields molar CO<sub>2</sub>/SO<sub>2</sub> of  $1.4 \pm 0.2$  and  $1.6 \pm 0.8$  respectively, i.e. without significant  
494 change in the ratio but with increase in uncertainty.

495

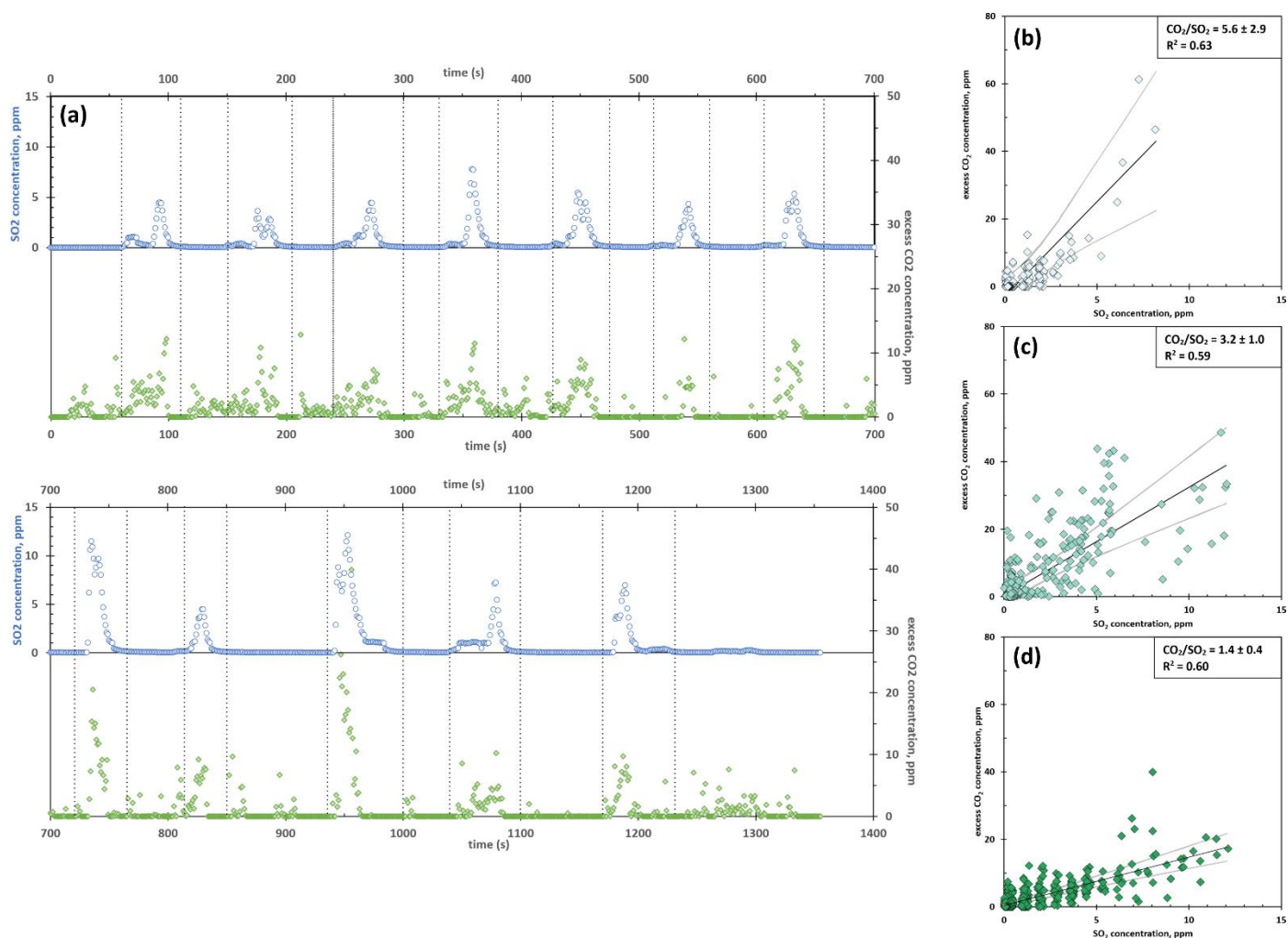
496

497  
498  
499



500  
501  
502  
503  
504  
505  
506  
507  
508  
509  
510  
511  
512

**Figure 5.** (a) The diamond-shaped data points show molar CO<sub>2</sub>/SO<sub>2</sub> ratios obtained for individual plume intercepts, coloured according to flight. The dashed horizontal lines show the weighted mean CO<sub>2</sub>/SO<sub>2</sub> ratio obtained by averaging the per-intercept ratios, with the weighting factor based on the per-intercept errors (shown by vertical bars on the diamonds). The shaded panels show the errors on these weighted means. (b) Molar CO<sub>2</sub>/SO<sub>2</sub> ratios obtained for each flight, calculated from linear regressions between SO<sub>2</sub> and excess CO<sub>2</sub> concentration data from all intercepts (Flight 4, n=5; Flight 5, n=9; Flight 6, n=12). Compare with per-flight weighted mean ratios shown by shaded bars in Figure 5a. (c) Molar CO<sub>2</sub>/SO<sub>2</sub> ratios obtained for individual plume intercepts, plotted against the corresponding maximum SO<sub>2</sub> concentration (ppm) measured during the intercept. (d) Molar CO<sub>2</sub>/SO<sub>2</sub> ratios obtained for individual plume intercepts, plotted against the duration of sensor exposure to the volcanic plume.



513  
514  
515  
516  
517  
518  
519

**Figure 6.** (a) Time series of SO<sub>2</sub> (blue) and excess CO<sub>2</sub> (green) concentrations measured by MultiGAS during intercepts of Bagana's plume during Flight 6, and correlation plots of SO<sub>2</sub> and excess CO<sub>2</sub> concentrations and molar CO<sub>2</sub>/SO<sub>2</sub> ratios for (b) Flight 4, (c) Flight 5 and (d) Flight 6. Black lines are the linear regressions from which we derive the ratios; grey lines show the 95% confidence intervals. Vertical grey dashed lines on the time series indicate the 'intercept' intervals (SO<sub>2</sub> concentration above the sensor noise) where the UAS flew through the volcanic plume, and which we used to derive per-intercept molar CO<sub>2</sub>/SO<sub>2</sub> ratios.

<b>Flight</b>	<b>Date, time</b> (GMT+11)	<b>Max SO<sub>2</sub>,</b> ppm	<b>Max excess CO<sub>2</sub>,</b> ppm	<b>CO<sub>2</sub>/SO<sub>2</sub></b>	<b>error</b>	<b>n*</b>	<b>Notes</b>	
<b>1</b>	16/09/20 17:45	-	-	-	-	-	Recon. flight without payload	
<b>2</b>	17/09/20 07:15	-	-	-	-	-	No plume interceptions	
<b>3</b>	17/09/20 08:50	6.2	3.0	-	-	-	Noisy CO <sub>2</sub> , did not analyse	
<b>4</b>	17/09/20 13:15	8.1	98.8	5.6	2.9	173	Five plume interceptions	
				2.5	8.1		Weighted mean intercepts 1-5	
<b>5</b>	18/09/20 06:45	12.0	72.8	3.2	1.0	468	Nine plume interceptions	
				5.9	1.5		341	<i>Intercepts 01-06 only</i>
				12.0	2.0		127	<i>Intercepts 07-08 only</i>
				4.3	2.2			Weighted mean intercepts 1-9
<b>6</b>	18/09/20 07:40	12.1	39.9	1.4	0.4	650	Twelve plume interceptions	
				7.8	0.6		376	<i>Intercepts 01-07 only</i>
				12.1	0.6		274	<i>Intercepts 08-12 only</i>
				1.3	0.2			Weighted mean intercepts 1-12
<b>7</b>	18/09/20 08:45	-	-	-	-	-	Abandoned flight due to rain	
<b>4-6<sup>‡</sup></b>	-	12.1	98.8	2.4	0.6	1311	Linear regression, 4-6	
				12.1	0.2		1311	Weighted mean, 4-6
				12.1	0.2		674	Weighted mean, 4-6 (SO <sub>2</sub> > 5 ppm)
				12.1	0.8		196	Weighted mean, 4-6 (SO <sub>2</sub> > 10 ppm)

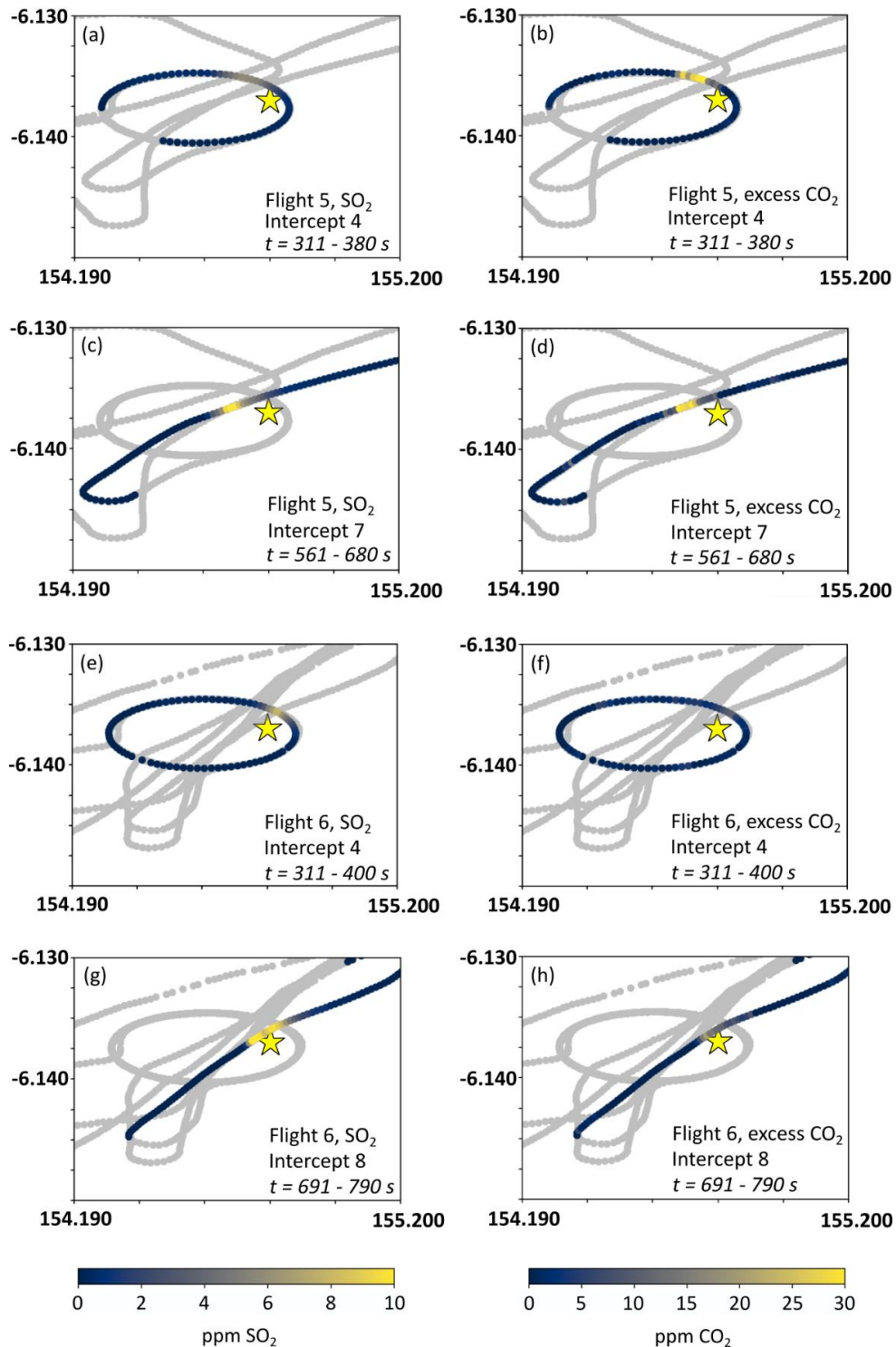
520

521

522

523

**Table 1.** Summary of our seven gas sensing flights with the Titan UAS. Date and time are in Bougainville local time. \*n is the number of measurements (at 1 Hz) used in the calculation of the ratios, effectively equal to the total duration of gas sensor contact with the volcanic plume (in seconds). <sup>‡</sup>This line refers to CO<sub>2</sub>/SO<sub>2</sub> ratios calculated by incorporating data from Flight 4, Flight 5 and Flight 6.



524 **Figure 7.** Gas concentrations measured by airborne MultiGAS in Flight 5, intercept 4 (a,b) and intercept 7 (c,d) and  
 525 Flight 6, intercept 4 (e,f) and intercept 8 (g,h). The grey lines show the full path of each flight; colours illustrate the  
 526 gas concentration, of SO<sub>2</sub> (a, c, e, g) and excess CO<sub>2</sub> (b, d, f, h). The yellow star represents the volcano's summit.  
 527 Each map covers the same area; all SO<sub>2</sub> panels and CO<sub>2</sub> panels respectively have consistent colour scales. The full  
 528 extent of gas sensing intervals (i.e. plume intercepts) from Flights 4-6 are shown in Supplementary Figure 4.

## 529            3.3 Sulfur Dioxide Emissions

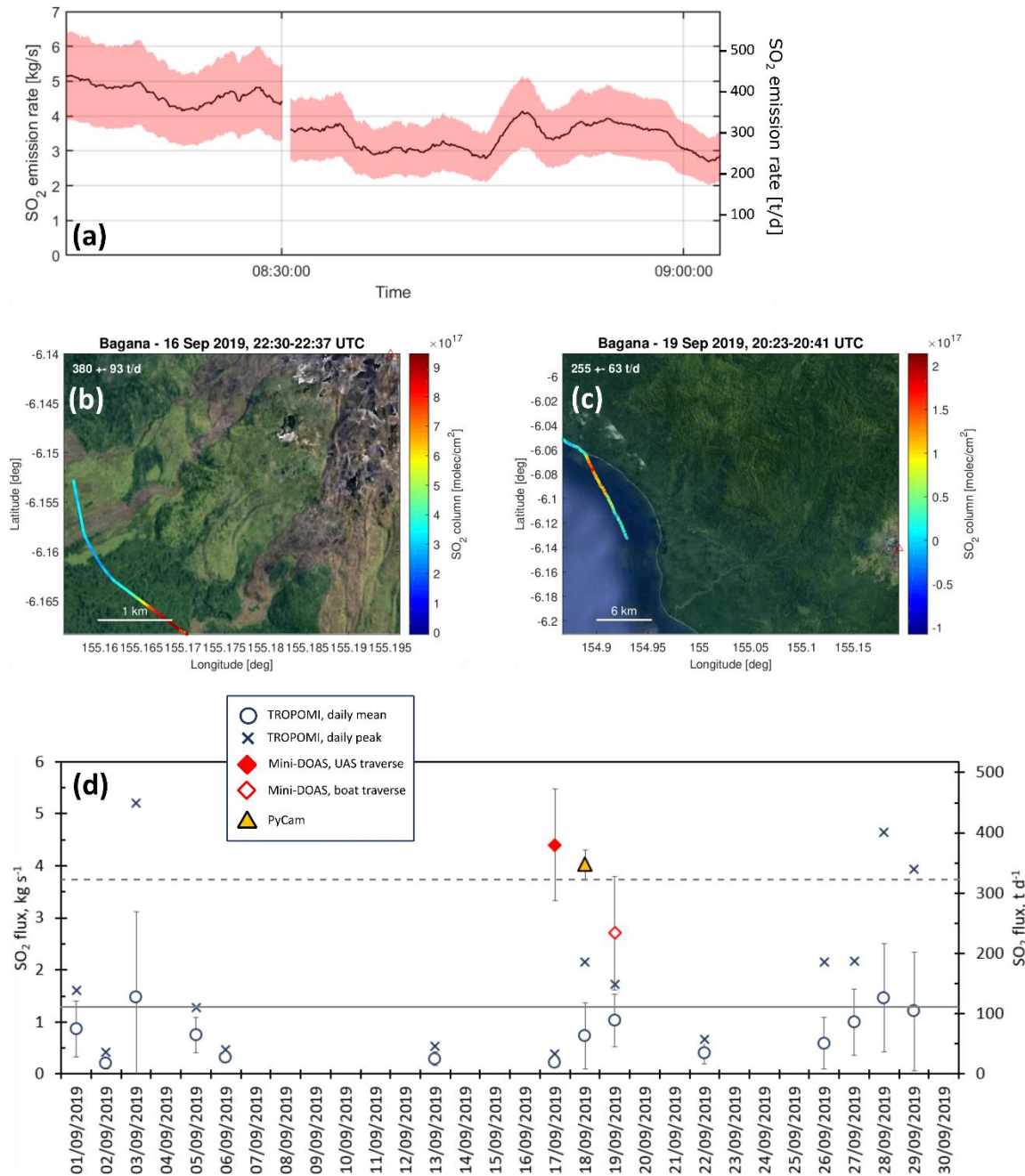
530    Our most reliable UV camera data comprises around one hour of measurements on the morning of  
531    18 September (first acquisition, 0805-0830; second acquisition 0835-0905) (Figure 8a). Despite  
532    relatively low UV levels due to the early time of day, clear skies prevailed over the volcano.  
533    Measurement attempts on the previous two days were thwarted by thick cloud cover, rain showers  
534    and weak SO<sub>2</sub> emissions.

535    We calculate mean ( $\pm$  standard deviation) SO<sub>2</sub> emission rates of  $4.65 \pm 0.28 \text{ kgs}^{-1}$  ( $401 \pm 24 \text{ td}^{-1}$ )  
536    in the first acquisition and  $3.37 \pm 0.37 \text{ kgs}^{-1}$  ( $292 \pm 32 \text{ td}^{-1}$ ) in the second (Figure 8a). The apparent  
537    decline in SO<sub>2</sub> flux through the observation period may be a volcanological phenomenon, though  
538    we observed no changes in activity, or a consequence of changing light levels influencing the  
539    instrument calibration.

540    We also measured SO<sub>2</sub> emissions using mini-DOAS spectrometer traverses (Figure 8b). When  
541    close to the volcano on 17 September, our UAS-mounted spectrometer failed to complete a full  
542    traverse of the plume. Despite this, we can estimate SO<sub>2</sub> emissions from a partial traverse at  $380$   
543     $\pm 92 \text{ td}^{-1}$ . If we assume that we captured the majority of the plume, this value should be within  
544    error of the true emission rate. As we were leaving the field area by boat on 20 September, we  
545    made zenith-pointing traverses with two mini-DOAS instruments. The plume was around 15 km  
546    wide at this distance ( $\sim 35 \text{ km}$ ) from the volcano summit. The resulting emission rates were  $251 \pm$   
547     $122 \text{ t/d}$  and  $234 \pm 94 \text{ t/d}$ , thus consistent with one another.

548

549  
550



551  
552  
553  
554  
555  
556  
557  
558  
559

**Figure 8.** (a) Time series of SO<sub>2</sub> flux from UV camera acquisition on morning of 18<sup>th</sup> September 2019, with one sigma uncertainty about the calculated flux value; (b) Maps of SO<sub>2</sub> vertical column density measured by mini-DOAS in traverses by multi-rotor UAS (left, 17<sup>th</sup> September 2019) and boat (right, 20<sup>th</sup> September 2019). (c) Composite daily SO<sub>2</sub> emission rate time series through September 2019, incorporating TROPOMI satellite observations and the ground-based remote sensing data we collected during our fieldwork. Horizontal dashed line shows the mean SO<sub>2</sub> emission rate from ground-based data; horizontal solid line shows the mean SO<sub>2</sub> emission rate from satellite-based data.

560

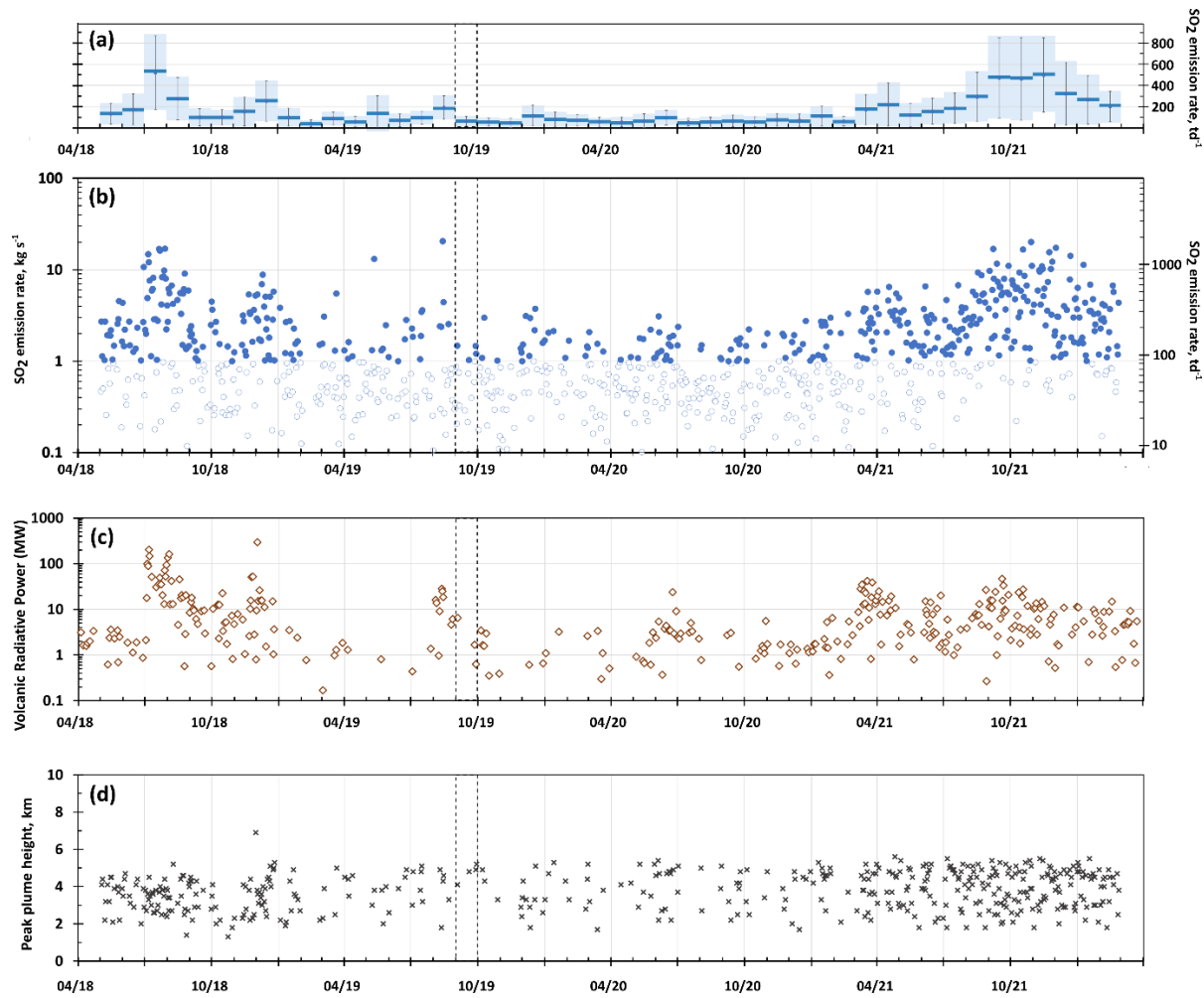
## 3.4 Satellite Observations of Gas and Thermal Emissions

561 TROPOMI observations allow us to quantify SO<sub>2</sub> emissions from May 2018 to February 2022  
562 (Figure 9, Figure 10, Supplementary Figure 5a-l). Over this interval, we obtained an estimate of  
563 mean daily SO<sub>2</sub> flux on 885 days, of which 453 days saw the mean flux exceed 1.0 kg s<sup>-1</sup>.  
564 TROPOMI failed to detect a plume from Bagana on 505 days, due either to emissions dropping  
565 below the sensor's resolution, cloud cover, or none of our PlumeTraj trajectories returning to  
566 Bagana. In September 2019, we have fourteen days with estimates of SO<sub>2</sub> flux, with an average of  
567 0.75 kg s<sup>-1</sup> (65 td<sup>-1</sup>) and a maximum peak daily flux of 5.20 kg s<sup>-1</sup> (450 td<sup>-1</sup>). Generally, our satellite-  
568 based emission rates in September 2019 are lower than those we measured by ground-based remote  
569 sensing in the field (Figure 8d). We are unable to evaluate rigorously whether this is due to  
570 different sensitivities, measurement geometries, or time or duration of measurement (i.e. satellite-  
571 based fluxes are constructed over several hours, our ground-based measurements each cover < 1  
572 hour). The mean ( $\pm$  S.D.) SO<sub>2</sub> emission rate in September 2019 if we combine our satellite and  
573 ground-based measurements is  $116 \pm 118$  td<sup>-1</sup>. This is lower than the mean of the ground-based  
574 measurements we made during our fieldwork and may be due to lower activity and emissions in  
575 the remainder of the month, or a low bias resulting from reduced TROPOMI sensitivity during  
576 periods of lower emissions (e.g. low altitudes, low vertical column densities).

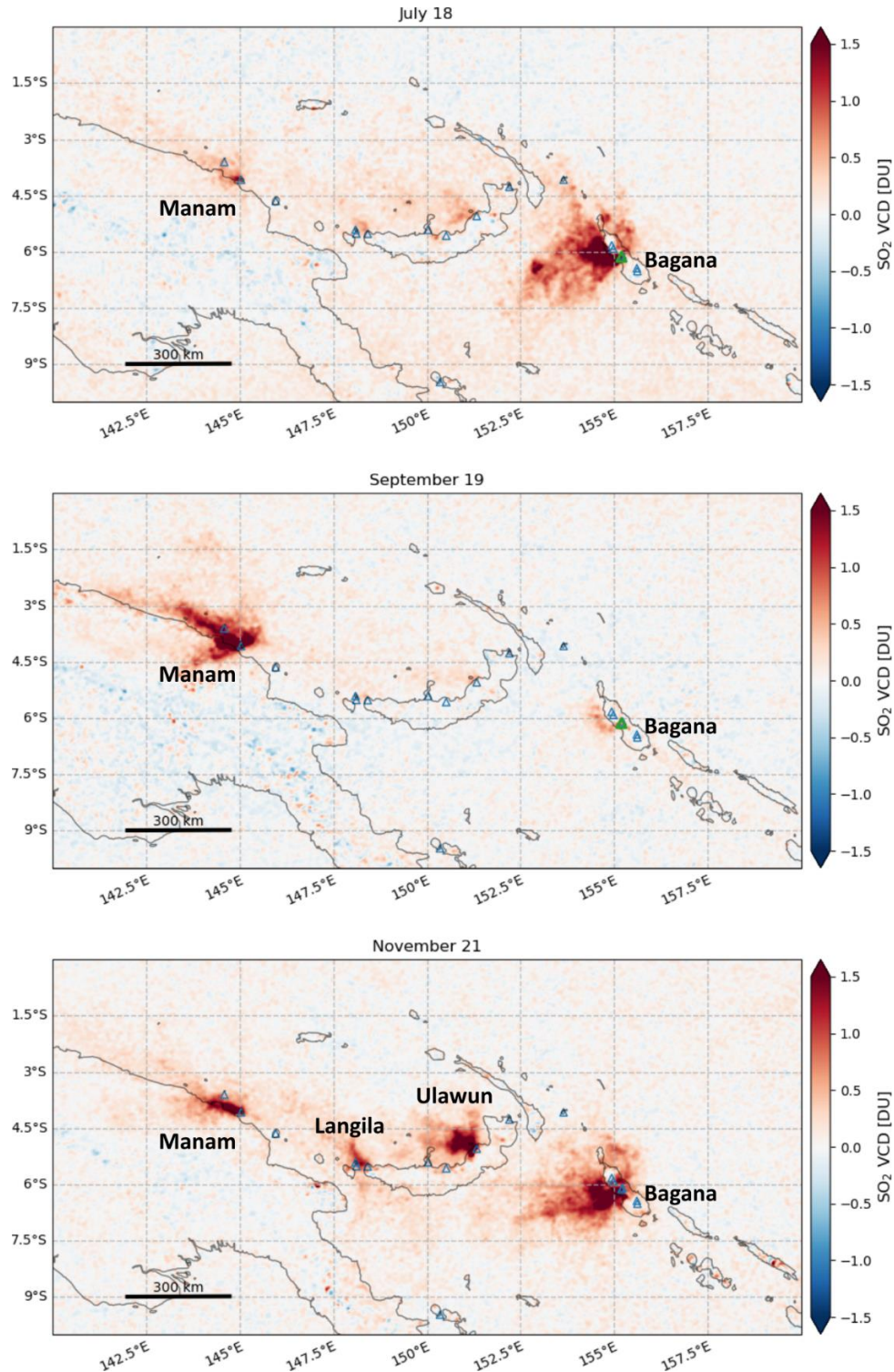
577 Our satellite observations suggest three broad phases of contrasting activity at Bagana since 2018:  
578 (i) from May to December 2018, SO<sub>2</sub> emissions are relatively high with mean ( $\pm$  S.D.) daily  
579 emissions per month ranging from  $100 \pm 70$  to  $520 \pm 348$  td<sup>-1</sup>; (ii) from January 2019 to March  
580 2021, SO<sub>2</sub> emissions are relatively low with mean daily emissions below 100 td<sup>-1</sup> in every month  
581 except August and December 2019; and (iii) since March 2021, SO<sub>2</sub> emissions are relatively high  
582 again, with mean daily emissions per month ranging from  $123 \pm 109$  to  $498 \pm 350$  td<sup>-1</sup> (Figure 9a).  
583 The large relative magnitude of the standard deviation to the mean points to high inter-daily  
584 variation in SO<sub>2</sub> emission rates (Figure 9b). Independent observations from the MODIS thermal  
585 infrared sensor, processed with the MIROVA algorithm (Coppola et al., 2016, 2020) support the  
586 notion of three periods of activity, with elevated thermal emissions in May-December 2018 and  
587 since March 2021, with an intervening period largely characterised by the absence of thermal  
588 emissions (Figure 9c). Peak SO<sub>2</sub> plume heights, another output of our PlumeTraj routine, do not  
589 show systematic variations with either SO<sub>2</sub> emission rate or thermal flux, but tend to lie between  
590 2-5 km for the entire study interval (Figure 9d).

591

592

593  
594595  
596  
597  
598  
599  
600  
601  
602  
603  
604

**Figure 9.** Satellite observations of Bagana's activity from May 2018 to present. (a) Mean ( $\pm$  standard deviation) SO<sub>2</sub> emission rate for each month of our study interval, derived from TROPOMI observations; (b) daily mean SO<sub>2</sub> emission rates retrieved from TROPOMI observations, with days where flux is below  $1.0 \text{ kg s}^{-1}$  ( $\sim 90 \text{ td}^{-1}$ ) and thus subject to greater uncertainty shown in paler colours; (c) volcanic radiative power, expressed in MW, obtained from the MIROVA system's analysis of MODIS thermal infrared retrievals over Bagana; (d) Maximum plume height retrieved per day, obtained from PlumeTraj analysis of TROPOMI retrievals. In each panel, the vertical black dashed lines highlight September 2019, when our fieldwork took place.



605 **Figure 10.** Average atmospheric SO<sub>2</sub> vertical column densities over Papua New Guinea, as observed by TROPOMI  
 606 for July 2018 (top), September 2019 (middle) and November 2021 (bottom). We construct these maps by averaging  
 607 all TROPOMI observations acquired in each month. In July 2018 and November 2021, Bagana was in a state of  
 608 active lava extrusion accompanied by elevated SO<sub>2</sub> gas emissions. In September 2019, coincident with our field  
 609 campaign, Bagana was in much lower state of activity (no visible eruption) and reduced gas emissions. Note SO<sub>2</sub>  
 610 emissions of varying strength from other volcanoes across the region: Manam, Langila and Ulawun.

611 **4 Discussion**

## 612 4.1 Carbon and Sulfur Fluxes from Bagana, and Implications for Regional Emissions Budgets

613 The molar CO<sub>2</sub>/SO<sub>2</sub> ratio for Bagana's plume is  $2.4 \pm 0.6$  if we calculate it via a single linear  
614 regression through all our MultiGAS data from Flights 4-6, or  $1.6 \pm 0.2$  if we calculate it via an  
615 error-weighted mean of our 26 per-intercept CO<sub>2</sub>/SO<sub>2</sub> ratios. The 'combined linear regression  
616 ratio' may obscure temporal variation in gas composition between each flight, while the 'error-  
617 weighted mean ratio' more explicitly accounts for temporal variations. Our error weighting of the  
618 mean compensates for the short duration of individual plume intercepts.

619 Our data (CO<sub>2</sub>/SO<sub>2</sub> =  $1.6 \pm 0.2$ ) suggest Bagana's gas emissions are carbon-poorer than, but  
620 overlap within error with, the composition (CO<sub>2</sub>/SO<sub>2</sub> =  $2.4 \pm 0.7$ ) predicted from global  
621 relationships between CO<sub>2</sub>/SO<sub>2</sub> in high temperature volcanic gas emissions and Ba/La (or Sr/Nd)  
622 in erupted rocks (Aiuppa et al., 2019). All Papua New Guinea's volcanoes, including Bagana, were  
623 assigned to 'Group 2', volcanoes characterised by relatively carbon-rich emissions due to efficient  
624 recycling of slab carbon into the sub-arc mantle. Whether this is true for Bagana remains open to  
625 debate. There are no direct samples of the subducting slab in the Solomon Sea (e.g. piston cores  
626 seaward of the Bougainville trench), just dredges and a free-fall grab from the *R.V. Natsushima's*  
627 1983-84 cruise (Crook, 1987; Woodhead et al., 1998). The sampled lithologies comprise  
628 volcanoclastic sediments, mudrocks and only minor limestones. It is not clear how well these  
629 samples reflect the slab composition at sub-arc depths. Trace element (e.g. Th/Yb vs Sr/Nd) and  
630 radiogenic isotope (i.e. Sr-Nd-Pb) data for lavas from Bagana and other Bougainville volcanoes  
631 suggest a fluid-dominated slab flux and only minor sedimentary influence (Hergt et al., 2018).  
632 This may explain our relatively carbon-poor gas compositions, but further work is required to  
633 characterise volatile provenance in this arc segment.

634 The gas composition predicted by Aiuppa et al. (2019) is based on the chemistry of lavas erupted  
635 over decades (Bultitude, 1982). Our data are direct measurements of Bagana's emissions but  
636 represent just two days of relatively low-level activity for this volcano. This considered, the fact  
637 the two estimates match within error is perhaps surprising. Volcanoes can exhibit dramatic  
638 temporal changes in gas composition, with CO<sub>2</sub>/SO<sub>2</sub> increasing following mafic recharge into  
639 shallow crustal reservoirs or as unrest builds prior to eruptions (e.g. Aiuppa et al., 2007; Werner  
640 et al., 2019). Our data do not allow us to predict whether Bagana's gas composition might vary as  
641 a function of activity, but it seems plausible that co-eruptive emissions may differ in composition  
642 to the gases we measured in September 2019, a period of relative quiescence. If we consider a  
643 general degassing model of andesitic volcanoes (e.g., Edmonds et al., 2022) that sees surface gas  
644 emissions as mixtures of deeply-exsolved (CO<sub>2</sub>-rich) fluids delivered largely through second  
645 boiling of intruded hydrous magmas, and more S-rich fluids released during shallow crystallization  
646 or ascent and extrusion, we may interpret our relatively low measured CO<sub>2</sub>/SO<sub>2</sub> as the product of  
647 residual degassing of shallow-stored magma that ascended to the upper reaches of Bagana's  
648 plumbing system but was not erupted. Thus, while our calculation of CO<sub>2</sub> emission rates relies on  
649 our measured CO<sub>2</sub>/SO<sub>2</sub> ratio, we note that this may not closely resemble Bagana's 'true' long-term  
650 gas composition.

651 We measured Bagana's SO<sub>2</sub> emission rate using a combination of a UAS traverse with mini-  
652 DOAS, a boat traverse with mini-DOAS, the PiCam, and TROPOMI satellite observations (Figure

653 8c). The mean ( $\pm$  standard deviation) SO<sub>2</sub> emission rate from our ground-based measurements  
654 (PiCam and mini-DOAS) is  $320 \pm 76$  td<sup>-1</sup>. These are the lowest emissions rates yet measured at  
655 Bagana. Earlier campaign measurements reported SO<sub>2</sub> fluxes of 3100 td<sup>-1</sup> in 1983 and 3200 td<sup>-1</sup> in  
656 1989, 1900 td<sup>-1</sup> in 2003, and 3900 td<sup>-1</sup> in 2016 (Global Volcanism Program, 1983, 1989;  
657 McGonigle et al., 2004; D'Aleo et al., 2017). Multi-year satellite observations have also suggested  
658 typical SO<sub>2</sub> emissions of  $\geq 10^3$  td<sup>-1</sup> from 2005-18 (Carn et al., 2017; McCormick Kilbride et al.,  
659 2019).

660 Since 2018, our new satellite observations suggest three intervals of differing behaviour, defined  
661 above in terms of SO<sub>2</sub> and thermal emissions as: (i) May to December 2018; (ii) January 2019 to  
662 March 2021; (iii) March 2021 to present. Our interpretation of these three intervals is that the first  
663 and third represent episodes of lava extrusion, while the second is a period of quiescence  
664 accompanied by passive SO<sub>2</sub> emissions (Figure 9). Elevated gas emissions accompanying active  
665 extrusion, interpreted from a striking correspondence between SO<sub>2</sub> and thermal emissions seems  
666 to be a characteristic feature of Bagana (Wadge et al., 2018; McCormick Kilbride et al., 2019) and  
667 is further evident in activity reports compiled by the Smithsonian Global Volcanism Program. The  
668 first interval of elevated gas and thermal emissions is likely to have coincided with the extrusion  
669 of the fresh lava flow we observed in Bagana's northern flank during our fieldwork in September  
670 2019. In spring 2021, thermal anomalies were detected by the Sentinel-2 satellite, initially confined  
671 to the summit area before spreading to the northern flank (Global Volcanism Program, 2021a,b).  
672 At the time of writing, we assume this lava extrusion may still be ongoing  
673 ([https://www.mirovaweb.it/?action=volcanoDetails\\_S2&volcano\\_id=255020](https://www.mirovaweb.it/?action=volcanoDetails_S2&volcano_id=255020)). Overall, our SO<sub>2</sub>  
674 data from September 2019 are consistent with the general decline in activity at Bagana since 2012  
675 (McCormick Kilbride et al., 2019; Global Volcanism Program, 2019a, 2019b, 2019c, 2020). The  
676 volcano exhibits a wide range in the intensity of its activity (further borne out by our satellite data  
677 in this study, Figure 9, Figure 10, Supplementary Figure 5a-l) and our field campaign coincided  
678 with a period of particularly low-level unrest.

679 The Bagana edifice is likely to be partly saturated with water, owing to heavy daily rainfall. There  
680 are numerous fumaroles on the summit rather than a single 'open vent', extensive mineral  
681 precipitation around these fumaroles, and faint odours of sulfur in the small rivers around the  
682 volcano (Figure 4c). However, we did not detect any H<sub>2</sub>S in the Bagana gas plume and therefore  
683 consider it unlikely that our SO<sub>2</sub> emission rates are strongly influenced by scrubbing (e.g.,  
684 Symonds et al., 2001).

685 A molar CO<sub>2</sub>/SO<sub>2</sub> ratio of  $1.6 \pm 0.2$  is equivalent to a mass ratio of  $1.1 \pm 0.1$ . Multiplying this by  
686 our mean ground-based SO<sub>2</sub> emission rate of  $320 \pm 76$  td<sup>-1</sup> yields a CO<sub>2</sub> flux of  $320 \pm 84$  td<sup>-1</sup>. This  
687 is our best estimate for Bagana's carbon emissions at the time of measurement in 2019, given the  
688 comparable temporal duration of our UAS-based plume composition data and our ground-based  
689 SO<sub>2</sub> emission rate data. Considering September 2019 as a whole, and our combined satellite plus  
690 ground-based SO<sub>2</sub> emission rate data, we estimate a CO<sub>2</sub> emission rate of  $128 \pm 130$  td<sup>-1</sup>. This  
691 estimate is subject to two key uncertainties, namely the assumption of fixed CO<sub>2</sub>/SO<sub>2</sub> throughout  
692 the month, and whether the ground- and satellite-based estimates of SO<sub>2</sub> emissions can be

693 seamlessly combined. The potential influence of these uncertainties only grows if we extrapolate  
694 our data over longer timescales.

695 We can calculate a long-term (i.e. multi-year) estimate of CO<sub>2</sub> emissions from Bagana by  
696 combining our campaign CO<sub>2</sub>/SO<sub>2</sub> (mass ratio of  $1.1 \pm 0.1$ ) with our mean ( $\pm$  standard deviation)  
697 SO<sub>2</sub> flux from TROPOMI observations in 2018-2022 ( $175 \pm 234$  td<sup>-1</sup>). The resulting value of CO<sub>2</sub>  
698 flux,  $193 \pm 257$  td<sup>-1</sup>, and our campaign-only value of  $320 \pm 84$  td<sup>-1</sup>, are significantly lower than the  
699 value of  $6245 \pm 2335$  td<sup>-1</sup> predicted by Aiuppa et al. (2019), who placed Bagana as Earth's fifth  
700 ranked volcanic carbon source. The CO<sub>2</sub>/SO<sub>2</sub> ratio ( $2.4 \pm 0.7$ , predicted as described above) and  
701 the SO<sub>2</sub> flux ( $1032$ - $1971$  kt yr<sup>-1</sup>, from satellite observations in 2005-15 presented by Carn et al.,  
702 2017) used by Aiuppa et al. (2019) in their computation of CO<sub>2</sub> flux are significantly higher than  
703 the values we measured in September 2019. Thus, our derived CO<sub>2</sub> emission rate is substantially  
704 lower and, in September 2019 at least, Bagana is unlikely to have been a significant contributor to  
705 global volcanic carbon emissions. During intervals of elevated activity, however, Bagana may  
706 indeed be one of Earth's most important volcanic carbon emitters. Fresh magmas fed into the  
707 shallow reservoirs from depth are likely to release relatively carbon-rich gas (with CO<sub>2</sub>/SO<sub>2</sub>  
708 perhaps comparable to Aiuppa et al. (2019)'s predicted value of  $2.4 \pm 0.7$ ). We know co-eruptive  
709 SO<sub>2</sub> fluxes at Bagana can exceed  $10^4$  td<sup>-1</sup> (this study, McCormick Kilbride et al., 2019, and  
710 references therein). Thus, peak CO<sub>2</sub> emissions at Bagana may be up to two orders of magnitude  
711 greater than what we measured in September 2019.

712 The foregoing discussion exemplifies a major challenge: how to accurately quantify global  
713 volcanic emissions when individual volcanoes have emissions that vary widely through time.  
714 Recent attempts to quantify global volcanic sulfur (Carn et al., 2017) and carbon emissions  
715 (Aiuppa et al., 2019; Werner et al., 2019; Fischer et al., 2019) partly agree with earlier studies (e.g.  
716 Andres & Kasgnoc, 1998) that certain volcanoes tend to rank highly from year to year, and from  
717 decade to decade. However, many other volcanoes once considered globally important sources of  
718 volatiles into the atmosphere are now exhibiting reduced activity and more modest emissions.  
719 Miyakejima, in the northern Izu-Bonin arc, was among the world's major SO<sub>2</sub> emitters following  
720 its effusive eruption in 2000 before an exponential drop in outgassing through the following decade  
721 (Kazahaya et al., 2004; Mori et al., 2013; Carn et al., 2017). Anatahan, in the Mariana arc, likewise  
722 retains a high ranking in global emissions inventories (Carn et al., 2017; Aiuppa et al., 2019),  
723 notwithstanding the fact that ~85% of its SO<sub>2</sub> flux over the past three decades coincided with short-  
724 lived, intense eruptions, mostly in January-August 2005 (McCormick et al., 2015). Kilauea  
725 volcano on Hawaii has been a prodigious source of gas into the atmosphere for decades, yet  
726 following the end of the 2018 East Rift Zone eruption, SO<sub>2</sub> emissions fell below  $100$  td<sup>-1</sup> (Elias et  
727 al., 2018; Kern et al., 2020). Conversely, Turrialba volcano in Costa Rica, awakened from a  
728 lengthy repose in 2018 and now dominates SO<sub>2</sub> and CO<sub>2</sub> emissions in the Central American  
729 Volcanic Arc (de Moor et al., 2017, c.f. Mather et al., 2006, and references therein). These data,  
730 and the picture of Bagana we present herein, illustrate that highly variable gas emission rates (and  
731 potentially composition, too) is inherent to many volcanoes and this fact could, and should, be  
732 better incorporated into volcanic emissions inventories.

733 Quantifying the temporal variability of volcanic emissions over longer timeframes is essential if  
734 we are to fully evaluate the influence of volcanic outgassing to the composition of Earth's  
735 atmosphere and consequently to planetary climate. The period of observations at volcanoes is still  
736 relatively short compared to the cycles of activity (Werner et al., 2019). Short duration campaign

737 datasets will seldom fully characterise highly dynamic systems and it follows that many volcanoes  
738 worldwide are inadequately characterised in terms of their outgassing flux and that many of our  
739 measurements are biased because they are often made during the most active periods (Werner et  
740 al., 2019). Long-term, more sustained and integrated emissions monitoring is required, melding  
741 synoptic satellite observations, automated ground-based remote sensing, permanently installed  
742 MultiGAS stations, regular sampling and analysis of emitted gases, and a key role for UAS in  
743 acquiring measurements and samples from otherwise inaccessible gas plumes (James et al., 2020;  
744 Edmonds, 2021; Kern et al., 2022).

745

#### 746 4.2 Aerial Strategies for Volcano Monitoring

747 Our UAS gas sensing flights have enabled the first measurements of gas composition and CO<sub>2</sub>  
748 outgassing from Bagana's otherwise inaccessible summit. The great potential of UAS in volcanic  
749 gas monitoring and research is evident (Stix et al., 2018; James et al., 2020; Liu et al., 2020a;  
750 Pering et al., 2020; Shinohara et al., 2020). In particular, flying beyond visual line of sight  
751 (BVLOS) enables safe access to volcanic plumes from a distance of several kilometres, removing  
752 the need to climb unstable edifices to access summit vents directly (Schellenberg et al., 2019; Liu  
753 et al., 2020a; Wood et al., 2020).

754 This study demonstrates that airborne MultiGAS measurements can recover volcanic plume gas  
755 composition robustly but challenges do remain. Our MultiGAS data sets are of shorter duration  
756 than ground-based studies, where the instrument may be exposed to gas for several days or  
757 installed permanently (e.g. Aiuppa et al., 2007, de Moor et al., 2016). Our instruments encountered  
758 relatively low gas concentrations over Bagana (c.f. our experience of a more 'open vent' system  
759 at Manam, Liu et al., 2020a) but this is an inherent feature of airborne sampling versus ground-  
760 based MultiGAS deployments (Werner et al., 2013; Fischer & Lopez, 2016). Multi-rotor aircraft,  
761 which can hover in place, may enable more sustained plume exposure however, multi-kilometre  
762 horizontal flight or ascent/descent with a multi-rotor are costly in terms of battery power, and the  
763 addition of more batteries greatly increases takeoff weight. The Titan cruises at roughly 20 ms<sup>-1</sup>  
764 which allowed us to reach the volcanic summit plume quickly and gliding back towards the landing  
765 site allowed us to expend more battery power over the summit, thus increasing plume exposure  
766 times. Thermal energy in buoyant volcanic plumes may help to extend endurance further by  
767 reducing power consumption during summit traverses (Wood et al., 2020). In future, vertical take-  
768 off and landing (VTOL) aircraft may offer a combination of the fixed-wing flight into a volcanic  
769 plume from a distance of several kilometres, accompanied by a relatively prolonged gas-sensing  
770 interval hovering in the plume. For now, potential uncertainties in gas composition arising from  
771 short sensor exposure to the volcanic gas can be overcome, as here, by repeated flights and by  
772 manual traverses within each flight to maximise gas contact. Through our three successful flights,  
773 increasing time spent in the plume did demonstrably lead to decreased uncertainty on our recovered  
774 CO<sub>2</sub>/SO<sub>2</sub> ratio (Figure 5b,d), although we cannot rule out that differences in the absolute value of  
775 the ratio from each flight are the result of spatial or temporal variations in gas composition.

776 Recovering UAS from distant and potentially turbulent airspace is no small feat, with changing  
777 volcanic activity potentially resulting in aircraft loss (Wood et al., 2020). Our work on Bagana  
778 directly followed our previous work on Manam and allowed us to explore our UAS capability

779 further. One challenge we experienced was a telemetry shadow when the volcanic edifice lay  
780 between our ground station and the aircraft. We modified the geometry of our flight plans to  
781 minimise the time that the Titan spent in this radio ‘dead zone’. We also flew closer to the volcanic  
782 summit than we had on Manam, at one point passing within 50 m altitude of the summit in pursuit  
783 of elevated gas concentrations. To achieve such close passes without aircraft loss requires high  
784 resolution and up-to-date topographic models for flight planning, which can be challenging to  
785 obtain for volcanoes with summit lava domes where active extrusion can modify topography by  
786 tens of metres. Moreover, a skilled pilot must monitor the in-flight FPV feed and take manual  
787 control in the event of turbulence or other threats to the aircraft. A full review of design  
788 requirements for successful fixed-wing UAS deployments is provided by Wood et al. (2020),  
789 resulting from volcanological fieldwork in recent years (Schellenberg et al., 2019; Liu et al.,  
790 2020a; this study).

791

#### 792 4.3 Future Volcano Monitoring at Bagana

793 Bagana is a remote volcano with no instrumented ground-based monitoring. A local observer  
794 provides regular radio reports of activity to Rabaul Volcanological Observatory (RVO) and  
795 community leaders liaise with the Bougainville Disaster Office (BDO) to discuss hazard mitigation  
796 and disaster risk reduction. The typical eruptive activity at Bagana, sluggish lava flows that are  
797 generally restricted to the cone, pose little direct hazard to populations in the surrounding villages  
798 (Figure 2). Of more concern are rare explosive eruptions which deposit hot ash on buildings,  
799 leading to fires and, more commonly, debris avalanches from the edifice into the upper reaches of  
800 the Torokina river.

801 In the absence of monitoring instruments, the main mitigation measures at Bagana are visits by  
802 RVO and BDO personnel to raise awareness among local communities of volcanic hazards. From  
803 our experience in the Wakovi and Piva communities, the level of hazard awareness is high among  
804 local people, with significant inter-generational memory of a range of activity styles. Moreover, a  
805 number of people described to us precursory phenomena they associate with imminent eruptions.  
806 This knowledge is among several factors influencing these communities’ resilience: strong kinship  
807 relations with adjacent communities ensure alternative dwelling places may be sought in times of  
808 elevated activity, and families can mobilise and evacuate quickly. The major caveat to this  
809 perspective is how the level of risk (and capacity for mitigation) might vary in more unusual  
810 activity, for example, the rare, high intensity explosive eruptions accompanied by pyroclastic flows  
811 known from Bagana’s eruptive history (Bultitude et al., 1978). It remains unknown why these  
812 events occur. Possibilities include mafic recharge introducing volatile-rich magma into the shallow  
813 plumbing system (e.g. Roberge et al., 2009), changes in supply of gas from deeper reservoirs into  
814 the shallow plumbing system (e.g., Liu et al., 2020b; Edmonds et al., 2022), or hydrothermal  
815 mineralisation sealing fractures in the summit dome and generating overpressure in the slowly  
816 degassing magma beneath (e.g., Heap et al., 2021). The scarcity of these events and therefore the  
817 limited experience of local communities in witnessing characteristic precursory behaviour  
818 increases community vulnerability. In our discussions with Wakovi residents, a recurring  
819 suggestion we heard was that the absence of a strong visible gas plume from Bagana’s summit  
820 would be perceived unusual or uncharacteristic and potentially taken as evidence of an imminent

821 eruption; this was usually illustrated via the analogy of a steaming cooking pot with a closely  
822 fitting lid.

823 The BVLOS measurements we describe herein require a skilled pilot and access to electronic  
824 components, so are not, in our judgment, yet feasible for regular monitoring in isolated locations  
825 such as the interior of Bougainville. Less complex UAS operations, such as deploying  
826 commercially available multi-rotor aircraft with onboard cameras for observations of changing  
827 unrest or edifice stability (e.g. accumulation of avalanche material on upper slopes) might be more  
828 feasible. Regular UAS-based surveillance and measurements of volcanic emissions have been  
829 recently adopted by RVO at other volcanoes, notably gas sensing flights at Rabaul and  
830 observations of the evolving lava flow hazard during the 2019 Ulawun flank fissure eruption. For  
831 now, a more realistic monitoring strategy for remote volcanoes in PNG may be the provision of  
832 satellite data to RVO, in near-real-time, that could be relayed to BDO or even communities in the  
833 Torokina region for dissemination to the surrounding villages. Such a strategy faces its own  
834 challenges, in terms of resourcing the regular analysis of satellite observations, timely and accurate  
835 transmission to RVO, data storage and processing capacity at the observatory, and reliable radio  
836 transmission to the remote interior of Bougainville. These challenges are set within a complex  
837 geopolitical context, with regional and national governments presently engaged in negotiations  
838 over the potential secession of Bougainville from Papua New Guinea. The foregoing discussion  
839 serves to illustrate the numerous challenges facing monitoring of remote volcanoes, particularly  
840 those capable of sustained eruptive activity, and also to emphasise the important and sometimes  
841 underappreciated role of local resilience measures in safeguarding populations from volcanic  
842 hazards..

843

844

845

846 **5 Conclusions**

847 We used UAS to fly a custom-built MultiGAS instrument into the summit plume of Bagana, a  
848 remote and persistently active volcano, and achieved the first measurements of the composition of  
849 Bagana gas emissions. We have demonstrated, building on our previous work, that fixed-wing  
850 UAS operating beyond visual line of sight are a powerful tool to study emissions from otherwise  
851 inaccessible vents. The short residence times we achieved in the plume (e.g. relative to  
852 conventional ground-based MultiGAS deployments) can be compensated for by repeated flights  
853 intercepting the plume. The uncertainties on our obtained plume composition data diminish with  
854 increased plume exposure, but such integration limits our ability to reconstruct temporal or spatial  
855 variations in gas composition. In future work, we aim to overcome these challenges, for example  
856 by developing aircraft that can hover or otherwise maintain prolonged contact between the gas  
857 sensor payload and the volcanic plume.

858 By combining our plume composition data with coincident remote sensing measurements of SO<sub>2</sub>  
859 emissions, we have derived a first estimate of CO<sub>2</sub> flux from Bagana, widely considered to be  
860 among Earth's major 'known unknown' sources of deep carbon into the atmosphere. Our  
861 fieldwork coincided with an interval of low-level activity at Bagana and our CO<sub>2</sub> emission rates  
862 were, accordingly, substantially lower than anticipated (200-320 td<sup>-1</sup> based on our data, versus a  
863 predicted flux of 6200 td<sup>-1</sup> by Aiuppa et al., 2019). Using multi-year satellite data, we have shown  
864 that Bagana's activity, like many volcanoes, is subject to wide temporal variations, and  
865 consequently outgassing rates vary widely too. Without any knowledge of the time dependence of  
866 plume composition (i.e. CO<sub>2</sub>/SO<sub>2</sub>), we argue that it is incorrect to extrapolate our short campaign  
867 data into longer term emissions estimates. In September 2019, Bagana was not likely to be among  
868 the major global volcanic carbon emitters. During intervals of elevated unrest, when both CO<sub>2</sub>/SO<sub>2</sub>  
869 ratio and SO<sub>2</sub> emissions are likely to be higher than our measurements, we might anticipate CO<sub>2</sub>  
870 emission rates of >10<sup>4</sup> td<sup>-1</sup>. A major challenge for the global volcanological research and  
871 monitoring community is how to capture variable gas composition at remote volcanoes or those  
872 otherwise without continuous or repeated measurements of gas chemistry. In the immediate term,  
873 long-term monitoring of such remote volcanoes as Bagana is to depend heavily on satellite  
874 observations, e.g. the SO<sub>2</sub> and thermal data we present here, with regular deployments of UAS  
875 potentially being made by local and regional observatory staff during periods of heightened unrest  
876 and threat.

877

878 **Acknowledgments**

879 BMK, EJM and AA acknowledge the financial support of the Alfred P Sloan foundation, awarded  
880 via the Deep Carbon Observatory. TR acknowledges funding via the CASCADE programme,  
881 EPSRC Programme Grant EP/R009953/1. CIS acknowledges the financial support of the New  
882 Zealand Earthquake Commission. The field team (BMK, EJM, KW, TCW, CIS, KM) are grateful  
883 to the Bougainville Disaster Office for logistical support and their valuable discussions around  
884 hazard and risk mitigation in the region, notably Michaelin Rave and colleagues for assistance in  
885 the field. We thank Alphonse and Sylton Vatsi for field support and are deeply grateful to Steven  
886 Naget and family, and all the people of Wakovi, for their warm hospitality, their assistance in  
887 traversing challenging terrain, and their insights into the historical and modern activity of  
888 Bagana. CH & MB acknowledge the UK Natural Environment Research Council funded V-  
889 PLUS project (NE/S004106/1). BMK acknowledges the NERC Centre for Observation and  
890 Modelling of Earthquakes, Volcanoes and Tectonics (COMET), which supported his first visit to  
891 Bagana and laid the groundwork for this study.

892

893

894 **Open Research**

895 Our data are stored in the Earthchem repository, specifically the DECADE portal which has recently  
896 been developed for the archival of volcanic gas data, including time series

897 (<https://earthchem.org/ecl/>). The data are archived at <https://doi.org/10.26022/IEDA/112898>.

898

899

900

901 **References**

902

903 Aiuppa, A., Federico, C., Giudice, G., Gurrieri, S. (2005). Chemical mapping of a fumarolic  
904 field: La Fossa Crater, Vulcano Island (Aeolian Islands, Italy). *Geophysical Research Letters*, 32  
905 (13), pp. 1-4.

906

907 Aiuppa, A., Moretti, R., Federico, C., Giudice, G., Gurrieri, S., Liuzzo, M., Papale, P.,  
908 Shinohara, H., Valenza, M. (2007) Forecasting Etna eruptions by real-time observation of  
909 volcanic gas composition. *Geology*, 35 (12), pp. 1115-1118.

910

911 Aiuppa, A., Bitetto, M., Francofonte, V., Velasquez, G., Parra, C.B., Giudice, G., Liuzzo, M.,  
912 Moretti, R., Moussallam, Y., Peters, N., Tamburello, G., Valderrama, O.A., Curtis, A. (2017). A  
913 CO<sub>2</sub>-gas precursor to the March 2015 Villarrica volcano eruption. *Geochemistry, Geophysics,*  
914 *Geosystems*, 18 (6), pp. 2120-2132.

915

916 Aiuppa, A., Fischer, T.P., Plank, T., Bani, P. (2019). CO<sub>2</sub> flux emissions from the Earth's most  
917 actively degassing volcanoes, 2005–2015. *Scientific Reports*, 9 (1), art. no. 5442.

918

919 Andres, R.J., Kasgnoc, A.D. (1998). A time-averaged inventory of subaerial volcanic sulfur  
920 emissions. *Journal of Geophysical Research Atmospheres*, 103 (D19), art. no. 98JD02091, pp.  
921 25251-25261.

922

923 Blake, D.H. (1968). Post miocene volcanoes on Bougainville Island, territory of Papua and New  
924 Guinea. *Bulletin Volcanologique*, 32 (1), pp. 121-138.

925

926 Bultitude, R. (1976). Eruptive history of Bagana volcano, Papua New Guinea, between 1882 and  
927 1975, *in* *Volcanism in Australasia*, ed R. Johnson (Amsterdam: Elsevier), 317–336

928

929 Bultitude, R.J. (1981) Literature search for pre-1945 sightings of volcanoes and their activity on  
930 Bougainville Island. Cooke-Ravian volume of volcanological papers, pp. 227-242.

931

932 Bultitude, R.J., Cooke, R.J.S. (1981) Note on activity from Bagana volcano from 1975 to 1980.  
933 Cooke-Ravian volume of volcanological papers, pp. 243-248.

934

935 Bultitude, R., Johnson, R., and Chappell, B. (1978). Andesites of Bagana volcano, Papua New  
936 Guinea: chemical stratigraphy, and a reference andesite composition. *BMR J. Aust. Geol.*  
937 *Geophys.* 3, 281–295.

938

939 Burton, M., Hayer, C., Miller, C., Christenson, B. (2021). Insights into the 9 December 2019  
940 eruption of Whakaari/White Island from analysis of TROPOMI SO<sub>2</sub> imagery. *Science Advances*,  
941 7 (25), art. no. eabg1218.

942

943 Campion, R., Delgado-Granados, H., Mori, T. (2015) Image-based correction of the light  
944 dilution effect for SO<sub>2</sub> camera measurements, *Journal of Volcanology and Geothermal Research*,  
945 300, pp48-57.

946

- 947 Carn, S.A., Fioletov, V.E., Mclinden, C.A., Li, C., Krotkov, N.A. (2017). A decade of global  
 948 volcanic SO<sub>2</sub> emissions measured from space. *Scientific Reports*, 7, art. no. 44095.  
 949
- 950 Coppola, D., Laiolo, M., Cigolini, C., Delle Donne, D., Ripepe, M. (2016). Enhanced volcanic  
 951 hot-spot detection using MODIS IR data: Results from the MIROVA system. *Geological Society*  
 952 *Special Publication*, 426 (1), pp. 181-205.  
 953
- 954 Coppola, D., Laiolo, M., Cigolini, C., Massimetti, F., Delle Donne, D., Ripepe, M., Arias, H.,  
 955 Barsotti, S., Parra, C.B., Centeno, R.G., Cevuard, S., Chigna, G., Chun, C., Garaebiti, E.,  
 956 Gonzales, D., Griswold, J., Juarez, J., Lara, L.E., López, C.M., Macedo, O., Mahinda, C.,  
 957 Ogburn, S., Prambada, O., Ramon, P., Ramos, D., Peltier, A., Saunders, S., de Zeeuw-van  
 958 Dalfsen, E., Varley, N., William, R. (2020). Thermal Remote Sensing for Global Volcano  
 959 Monitoring: Experiences From the MIROVA System. *Frontiers in Earth Science*, 7, art. no. 362.  
 960
- 961 Crook, K.A.W. (1987). Petrology and mineral chemistry of sedimentary rocks from the Western  
 962 Solomon Sea, *Geo-Marine Letters*, 6 (4), pp. 203-209.  
 963
- 964 D'Aleo R, McCormick B, Salem L, Edmonds M, Bitetto M, Tamburello G, Fischer T, Barry P,  
 965 Galle B, Arellano S, Mulina K, Itikarai I, Wallius J, Aiuppa A. 2017. Preliminary results of a  
 966 multi-parametric characterisation of gas manifestations from volcanoes in west Papua New  
 967 Guinea. *Conferenza Rittmann Giovani Ricercatori, 2017*.  
 968
- 969 de Moor, J.M., Aiuppa, A., Avar, G., Wehrmann, H., Dunbar, N., Muller, C., Tamburello, G.,  
 970 Giudice, G., Liuzzo, M., Moretti, R., Conde, V., Galle, B. (2016). Turmoil at Turrialba Volcano  
 971 (Costa Rica): Degassing and eruptive processes inferred from high-frequency gas monitoring.  
 972 *Journal of Geophysical Research: Solid Earth*, 121 (8), pp. 5761-5775.  
 973
- 974 de Moor, J.M., Kern, C., Avar, G., Muller, C., Aiuppa, A., Saballos, A., Ibarra, M., LaFemina,  
 975 P., Protti, M., Fischer, T.P. (2017). A New Sulfur and Carbon Degassing Inventory for the  
 976 Southern Central American Volcanic Arc: The Importance of Accurate Time-Series Data Sets  
 977 and Possible Tectonic Processes Responsible for Temporal Variations in Arc-Scale Volatile  
 978 Emissions. *Geochemistry, Geophysics, Geosystems*, 18 (12), pp. 4437-4468.  
 979
- 980 Draxler, R.R., and G.D. Hess, 1998: An overview of the HYSPLIT\_4 modeling system of  
 981 trajectories, dispersion, and deposition. *Aust. Meteor. Mag.*, 47, 295-308.  
 982
- 983 Edmonds, M. (2021). Geochemical monitoring of volcanoes and the mitigation of volcanic gas  
 984 hazards. In: *Forecasting and Planning for Volcanic Hazards, Risks, and Disasters* (ed. Papale,  
 985 P.), Elsevier.  
 986
- 987 Edmonds, M., Liu, E.J., Cashman, K.V. (2022). Open-vent volcanoes fuelled by depth-integrated  
 988 magma degassing. *Bulletin of Volcanology*, 84 (3), art. no. 28.  
 989
- 990 Fischer, T.P., Arellano, S., Carn, S., Aiuppa, A., Galle, B., Allard, P., Lopez, T., Shinohara, H.,  
 991 Kelly, P., Werner, C., Cardellini, C., Chiodini, G. (2019). The emissions of CO<sub>2</sub> and other  
 992 volatiles from the world's subaerial volcanoes. *Scientific Reports*, 9 (1), art. no. 18716.

- 993  
994 Fischer, T.P. & T.M. Lopez. (2016). First airborne samples of a volcanic plume for  $\delta^{13}\text{C}$  of  $\text{CO}_2$   
995 determinations. *Geophysical Research Letters*, 43 (7).  
996
- 997 Galle, B., Oppenheimer, C., Geyer, A., McGonigle, A.J.S., Edmonds, M., Horrocks, L. (2003). A  
998 miniaturised ultraviolet spectrometer for remote sensing of  $\text{SO}_2$  fluxes: A new tool for volcano  
999 surveillance. *Journal of Volcanology and Geothermal Research*, 119 (1-4), pp. 241-254.  
1000
- 1001 Gliß, J., Stebel, K., Kylling, A., Dinger, A.S., Sihler, H., Sudbø, A. (2017). Pyplis—a python  
1002 software toolbox for the analysis of  $\text{SO}_2$  camera images for emission rate retrievals from point  
1003 sources. *Geosciences (Switzerland)*, 7 (4), art. no. 134.  
1004
- 1005 Global Volcanism Program, 1983. Report on Bagana (Papua New Guinea) (McClelland, L., ed.).  
1006 *Scientific Event Alert Network Bulletin*, 8:9. Smithsonian Institution.  
1007 <https://doi.org/10.5479/si.GVP.SEAN198309-255020>.  
1008 Global Volcanism Program, 1989. Report on Bagana (Papua New Guinea) (McClelland, L., ed.).  
1009 *Scientific Event Alert Network Bulletin*, 14:7. Smithsonian Institution.  
1010 <https://doi.org/10.5479/si.GVP.SEAN198907-255020>.  
1011 Global Volcanism Program, 2019a. Report on Bagana (Papua New Guinea) (Venzke, E., ed.).  
1012 *Bulletin of the Global Volcanism Network*, 50:1. Smithsonian Institution.  
1013 <https://doi.org/10.5479/si.GVP.BGVN201902-255020>  
1014
- 1015 Global Volcanism Program, 2019b. Report on Bagana (Papua New Guinea) (Crafford, A.E., and  
1016 Venzke, E., eds.). *Bulletin of the Global Volcanism Network*, 44:6. Smithsonian Institution.  
1017 <https://doi.org/10.5479/si.GVP.BGVN201906-255020>  
1018
- 1019 Global Volcanism Program, 2019c. Report on Bagana (Papua New Guinea) (Bennis, K.L., and  
1020 Venzke, E., eds.). *Bulletin of the Global Volcanism Network*, 44:12. Smithsonian Institution.  
1021 <https://doi.org/10.5479/si.GVP.BGVN201912-255020>  
1022
- 1023 Global Volcanism Program, 2020. Report on Bagana (Papua New Guinea) (Venzke, E., ed.).  
1024 *Bulletin of the Global Volcanism Network*, 45:7. Smithsonian Institution.  
1025 <https://doi.org/10.5479/si.GVP.BGVN202007-255020>  
1026
- 1027 Global Volcanism Program, 2021a. Report on Bagana (Papua New Guinea) (Bennis, K.L., and  
1028 Venzke, E., eds.). *Bulletin of the Global Volcanism Network*, 46:1. Smithsonian Institution.  
1029 <https://doi.org/10.5479/si.GVP.BGVN202101-255020>  
1030
- 1031 Global Volcanism Program, 2021b. Report on Bagana (Papua New Guinea) (Bennis, K.L., and  
1032 Venzke, E., eds.). *Bulletin of the Global Volcanism Network*, 46:9. Smithsonian Institution.  
1033
- 1034 Hergt J, Woodhead J, Johnson RW. 2018. Potassium enrichment in arc lavas: a case study from  
1035 Bougainville Island. *State of the Arc conference 2018*.  
1036
- 1037 Holm, R.J., Rosenbaum, G., Richards, S.W. (2016). Post 8 Ma reconstruction of Papua New  
1038 Guinea and Solomon Islands: Microplate tectonics in a convergent plate boundary setting. *Earth-*

1039 Science Reviews, 156, pp. 66-81.

1040

1041 James, M.R., Carr, B.B., D'Arcy, F., Diefenbach, A.K., Dietterich, H.R., Fornaciai, A., Lev, E.,  
1042 Liu, E.J., Pieri, D.C., Rodgers, M., Smets, B., Terada, A., von Aulock, F.W., Walter, T.R.,  
1043 Wood, K.T., Zorn, E.U.

1044 (2020). Volcanological applications of unoccupied aircraft systems (UAS): Developments,  
1045 strategies, and future challenges. *Volcanica*, 3 (1), pp. 64-114.

1046

1047 Kantzas, E.P., McGonigle, A.J.S., Tamburello, G., Aiuppa, A., Bryant, R.G. (2010). Protocols  
1048 for UV camera volcanic SO<sub>2</sub> measurements. *Journal of Volcanology and Geothermal Research*,  
1049 194 (1-3), pp. 55-60.

1050

1051 Kazahaya, K., Shinohara, H., Uto, K., Odai, M., Nakahori, Y., Mori, H., Iino, H., Miyashita, M.,  
1052 Hirabayashi, J. (2004). Gigantic SO<sub>2</sub> emission from Miyakejima volcano, Japan, caused by  
1053 caldera collapse. *Geology*, 32 (5), pp. 425-428.

1054

1055 Kazahaya, R., Shinohara, H., Ohminato, T., Kaneko, T. (2019). Airborne measurements of  
1056 volcanic gas composition during unrest at Kuchinoerabujima volcano, Japan. *Bulletin of*  
1057 *Volcanology*, 81 (2), art. no. 7.

1058

1059 Kern, C., Lerner, A.H., Elias, T., Nadeau, P.A., Holland, L., Kelly, P.J., Werner, C.A., Clor,  
1060 L.E., Cappos, M. (2020). Quantifying gas emissions associated with the 2018 rift eruption of  
1061 Kīlauea Volcano using ground-based DOAS measurements. *Bulletin of Volcanology*, 82 (7), art.  
1062 no. 55.

1063

1064 Kern, C., Aiuppa, A., de Moor, J.M. (2022). A golden era for volcanic gas geochemistry?  
1065 *Bulletin of Volcanology*, 84 (5), art. no. 43.

1066

1067 Kern, C., Deutschmann, T., Werner, C., Sutton, A.J., Elias, T., Kelly, P.J. (2012). Improving the  
1068 accuracy of SO<sub>2</sub> column densities and emission rates obtained from upward-looking UV-  
1069 spectroscopic measurements of volcanic plumes by taking realistic radiative transfer into  
1070 account. *Journal of Geophysical Research Atmospheres*, 117 (20), art. no. D20302.

1071

1072 Liu, E.J., Wood, K., Mason, E., Edmonds, M., Aiuppa, A., Giudice, G., Bitetto, M., Francofonte,  
1073 V., Burrow, S., Richardson, T., Watson, M., Pering, T.D., Wilkes, T.C., McGonigle, A.J.S.,  
1074 Velasquez, G., Melgarejo, C., Bucarey, C. (2019). Dynamics of Outgassing and Plume Transport  
1075 Revealed by Proximal Unmanned Aerial System (UAS) Measurements at Volcán Villarrica,  
1076 Chile. *Geochemistry, Geophysics, Geosystems*, 20 (2), pp. 730-750.

1077

1078 Liu, E.J., Aiuppa, A., Alan, A., Arellano, S., Bitetto, M., Bobrowski, N., Carn, S., Clarke, R.,  
1079 Corrales, E., De Moor, J.M., Diaz, J.A., Edmonds, M., Fischer, T.P., Freer, J., Fricke, G.M.,  
1080 Galle, B., Gerdes, G., Giudice, G., Gutmann, A., Hayer, C., Itikarai, I., Jones, J., Mason, E.,  
1081 McCormick Kilbride, B.T., Mulina, K., Nowicki, S., Rahilly, K., Richardson, T., Rüdiger, J.,  
1082 Schipper, C.I., Watson, I.M., Wood, K. (2020).

1083 Aerial strategies advance volcanic gas measurements at inaccessible, strongly degassing  
1084 volcanoes

- 1085 (2020a) *Science Advances*, 6 (44), art. no. abb9103.  
1086
- 1087 Liu, E.J., Cashman, K.V., Miller, E., Moore, H., Edmonds, M., Kunz, B.E., Jenner, F., Chigna,  
1088 G. (2020b).  
1089 Petrologic monitoring at Volcán de Fuego, Guatemala. *Journal of Volcanology and Geothermal*  
1090 *Research*, 405, art. no. 107044.  
1091
- 1092 Massimetti F, Coppola D, Laiola M, Valade S, Cigolini C, Ripepe M, (2020). Volcanic Hot-Spot  
1093 detection using SENTINEL-2: A comparison with MODIS-MIROVA thermal data series.  
1094 *Remote Sensing*, 12 (5).  
1095
- 1096 Mather, T.A., Pyle, D.M., Tsanev, V.I., McGonigle, A.J.S., Oppenheimer, C., Allen, A.G.  
1097 (2006). A reassessment of current volcanic emissions from the Central American arc with  
1098 specific examples from Nicaragua. *Journal of Volcanology and Geothermal Research*, 149 (3-4),  
1099 pp. 297-311.  
1100
- 1101 McCormick, B., Popp, C., Andrews, B., Cottrell, E. (2015). Ten years of satellite observations  
1102 reveal highly variable sulphur dioxide emissions at Anatahan Volcano, Mariana Islands. *Journal*  
1103 *of Geophysical Research*, 120 (14), pp. 7258-7282.  
1104
- 1105 McCormick, B.T., Edmonds, M., Mather, T.A., Carn, S.A. (2012). First synoptic analysis of  
1106 volcanic degassing in Papua New Guinea. *Geochemistry, Geophysics, Geosystems*, 13 (3), art.  
1107 no. 7.  
1108
- 1109 McCormick Kilbride, B.T., Mulina, K., Wadge, G., Johnson, R.W., Itikarai, I., Edmonds, M.  
1110 (2019).  
1111 Multi-year satellite observations of sulfur dioxide gas emissions and lava extrusion at Bagana  
1112 volcano, Papua New Guinea, *Frontiers in Earth Science*, 7, art. no. 9.
- 1113 McGonigle, A.J.S., Oppenheimer, C., Tsanev, V.I., Saunders, S., Mulina, K., Tohui, S., Bosco,  
1114 J., Nahou, J., Kuduon, J., Taranu, F. (2004). Sulphur dioxide fluxes from Papua New Guinea's  
1115 volcanoes. *Geophysical Research Letters*, 31 (8), pp. L08606 1-4.  
1116
- 1117 McGonigle, A.J.S., Aiuppa, A., Giudice, G., Tamburello, G., Hodson, A.J., Gurrieri, S. (2008).  
1118 Unmanned aerial vehicle measurements of volcanic carbon dioxide fluxes. *Geophysical*  
1119 *Research Letters*, 35 (6), art. no. L06303.  
1120
- 1121 Mori, T., Burton, M. (2006). The SO<sub>2</sub> camera: A simple, fast and cheap method for ground-  
1122 based imaging of SO<sub>2</sub> in volcanic plumes. *Geophysical Research Letters*, 33 (24), art. no.  
1123 L24804.  
1124
- 1125 Mori, T., Shinohara, H., Kazahaya, K., Hirabayashi, J.-I., Matsushima, T., Mori, T., Ohwada,  
1126 M., Odai, M., Iino, H., Miyashita, M. (2013). Time-averaged SO<sub>2</sub> fluxes of subduction-zone  
1127 volcanoes: Example of a 32-year exhaustive survey for Japanese volcanoes. *Journal of*  
1128 *Geophysical Research Atmospheres*, 118 (15), pp. 8662-8674.  
1129

- 1130 Pering, T.D., Liu, E.J., Wood, K., Wilkes, T.C., Aiuppa, A., Tamburello, G., Bitetto, M.,  
1131 Richardson, T., McGonigle, A.J.S. (2020). Combined ground and aerial measurements resolve  
1132 vent-specific gas fluxes from a multi-vent volcano. *Nature Communications*, 11 (1), art. no.  
1133 3039.
- 1134  
1135 Queißer, M., Burton, M., Theys, N., Pardini, F., Salerno, G., Caltabiano, T., Varnam, M., Esse,  
1136 B., Kazahaya, R. (2019). TROPOMI enables high resolution SO<sub>2</sub> flux observations from Mt.  
1137 Etna, Italy, and beyond. *Scientific Reports*, 9 (1), art. no. 957.
- 1138  
1139 Roberge, J., Delgado-Granados, H., Wallace, P.J. (2009). Mafic magma recharge supplies high  
1140 CO<sub>2</sub> and SO<sub>2</sub> gas fluxes from Popocatepetl volcano, Mexico. *Geology*, 37 (2), pp. 107-110.
- 1141  
1142 Rüdiger, J., Tirpitz, J.-L., Maarten De Moor, J., Bobrowski, N., Gutmann, A., Liuzzo, M., Ibarra,  
1143 M., Hoffmann, T. (2018). Implementation of electrochemical, optical and denuder-based sensors  
1144 and sampling techniques on UAV for volcanic gas measurements: Examples from Masaya,  
1145 Turrialba and Stromboli volcanoes. *Atmospheric Measurement Techniques*, 11 (4), pp. 2441-  
1146 2457.
- 1147  
1148 Schellenberg, B., Richardson, T., Watson, M., Greatwood, C., Clarke, R., Thomas, R., Wood, K.,  
1149 Freer, J., Thomas, H., Liu, E., Salama, F., Chigna, G. (2019). Remote sensing and identification  
1150 of volcanic plumes using fixed-wing UAVs over Volcán de Fuego, Guatemala. *Journal of Field  
1151 Robotics*, 36 (7), pp. 1192-1211.
- 1152  
1153 Shinohara, H., Kazahaya, R., Ohminato, T., Kaneko, T., Tsunogai, U., Morita, M. (2020).  
1154 Variation of volcanic gas composition at a poorly accessible volcano: Sakurajima, Japan. *Journal  
1155 of Volcanology and Geothermal Research*, 407, art. no. 107098.
- 1156  
1157 Stix, J., de Moor, J.M., Rüdiger, J., Alan, A., Corrales, E., D'Arcy, F., Diaz, J.A., Liotta, M.  
1158 (2018).  
1159 Using Drones and Miniaturized Instrumentation to Study Degassing at Turrialba and Masaya  
1160 Volcanoes, Central America. *Journal of Geophysical Research: Solid Earth*, 123 (8), pp. 6501-  
1161 6520.
- 1162  
1163 Symonds, R.B., Gerlach, T.M., Reed, M.H. (2001). Magmatic gas scrubbing: Implications for  
1164 volcano monitoring. *Journal of Volcanology and Geothermal Research*, 108 (1-4), pp. 303-341.
- 1165  
1166 Tamburello, G. (2015). Ratiocalc: Software for processing data from multicomponent volcanic  
1167 gas analyzers. *Computers and Geosciences*, 82, pp. 63-67.
- 1168  
1169 Theys, N., Hedelt, P., De Smedt, I., Lerot, C., Yu, H., Vlietinck, J., Pedernana, M., Arellano, S.,  
1170 Galle, B., Fernandez, D., Carlito, C.J.M., Barrington, C., Taisne, B., Delgado-Granados, H.,  
1171 Loyola, D., Van Roozendaal, M. (2019). Global monitoring of volcanic SO<sub>2</sub> degassing with  
1172 unprecedented resolution from TROPOMI onboard Sentinel-5 Precursor. *Scientific Reports*, 9  
1173 (1), art. no. 2643.
- 1174  
1175

- 1176 Theys, N., Fioletov, V., Li, C., De Smedt, I., Lerot, C., McLinden, C., Krotkov, N., Griffin, D.,  
 1177 Clarisse, L., Hedelt, P., Loyola, D., Wagner, T., Kumar, V., Innes, A., Ribas, R., Hendrick, F.,  
 1178 Vlietinck, J., Brenot, H., Van Roozendael, M. (2021). A sulfur dioxide Covariance-Based  
 1179 Retrieval Algorithm (COBRA): application to TROPOMI reveals new emission sources.  
 1180 *Atmospheric Chemistry & Physics*, 21, pp. 16727–16744, [https://doi.org/10.5194/acp-21-16727-](https://doi.org/10.5194/acp-21-16727-2021)  
 1181 [2021](https://doi.org/10.5194/acp-21-16727-2021).  
 1182
- 1183 Veefkind, J.P., Aben, I., McMullan, K., Förster, H., de Vries, J., Otter, G., Claas, J., Eskes, H.J.,  
 1184 de Haan, J.F., Kleipool, Q., van Weele, M., Hasekamp, O., Hoogeveen, R., Landgraf, J., Snel,  
 1185 R., Tol, P., Ingmann, P., Voors, R., Kruizinga, B., Vink, R., Visser, H., Levelt, P.F. (2012).  
 1186 TROPOMI on the ESA Sentinel-5 Precursor: A GMES mission for global observations of the  
 1187 atmospheric composition for climate, air quality and ozone layer applications. *Remote Sensing*  
 1188 *of Environment*, 120, pp. 70-83.  
 1189
- 1190 Wadge, G., Saunders, S., Itikarai, I. (2012). Pulsatory andesite lava flow at Bagana Volcano.  
 1191 *Geochemistry, Geophysics, Geosystems*, 13 (11), art. no. Q11011.  
 1192
- 1193 Wadge, G., McCormick Kilbride, B.T., Edmonds, M., Johnson, R.W. (2018). Persistent growth  
 1194 of a young andesite lava cone: Bagana volcano, Papua New Guinea. *Journal of Volcanology and*  
 1195 *Geothermal Research*, 356, pp. 304-315.  
 1196
- 1197 Werner C, Kelly PJ, Doukas M, Lopez T, Pfeffer M, McGimsey R, Neal C. (2013). Degassing of  
 1198 CO<sub>2</sub>, SO<sub>2</sub>, and H<sub>2</sub>S associated with the 2009 eruption of Redoubt Volcano, Alaska. *Journal of*  
 1199 *Volcanology and Geothermal Research*, 259.  
 1200
- 1201 Werner C, Fischer T, Aiuppa A., Edmonds M, Cardellini C, Carn S, Chiodini G, Cottrell E,  
 1202 Burton M, Shinohara H, Allard P. 2019. Carbon dioxide emissions from subaerial volcanic  
 1203 regions: two decades in review. *In: Deep Carbon: Past to Present* (ed. Orcutt B, Daniel I,  
 1204 Dasgupta R), Cambridge University Press.  
 1205
- 1206 Wilkes, T.C., McGonigle, A.J.S., Pering, T.D., Taggart, A.J., White, B.S., Bryant, R.G.,  
 1207 Willmott, J.R. (2016). Ultraviolet imaging with low cost smartphone sensors: Development and  
 1208 application of a raspberry pi-based UV camera. *Sensors (Switzerland)*, 16 (10), art. no. 1649.  
 1209
- 1210 Wilkes, T.C., Pering, T.D., McGonigle, A.J.S., Tamburello, G., Willmott, J.R. (2017). A low-  
 1211 cost smartphone sensor-based UV camera for volcanic SO<sub>2</sub> emission measurements. *Remote*  
 1212 *Sensing*, 9 (1), art. no. 27.  
 1213
- 1214 Wood, K., et al. (2019). A deconvolution-based sensor response correction for volcanic gas  
 1215 measurements, Poster F41, Deep Carbon 2019, Washington, D.C.  
 1216
- 1217 Wood, K., Liu, E.J., Richardson, T., Clarke, R., Freer, J., Aiuppa, A., Giudice, G., Bitetto, M.,  
 1218 Mulina, K., Itikarai, I. (2020). BVLOS UAS Operations in Highly-Turbulent Volcanic Plumes.  
 1219 *Frontiers in Robotics and AI*, 7, art. no. 549716.  
 1220

1221 Woodhead, J.D., Eggins, S.M., Johnson, R.W. (1998). Magma genesis in the New Britain island  
1222 arc: further insights into melting and mass transfer processes. *Journal of Petrology*, 39 (9), pp.  
1223 1641-1668.  
1224  
1225  
1226